VOLUME IIB

TECHNICAL SUBSTANTIATION

THREE-DIMENSIONAL CHARACTERISTICS

This volume is a 1984 effort. There is no art work and the hand printed tables were employed to conserve time. The masters are the typed pages and hand drawn figures stored with the masters for the other volumes in the Naval Ship Systems area.

VOLUME IIB

THREE DIMENSIONAL CHARACTERISTICS

CONTENTS

CONTENTS (contd.)

CONTENTS (contd.)

CONTENTS (contd.)

ILLUSTRATIONS

ILLUSTRATIONS (contd.)

ILLUSTRATIONS (contd.)

TABLES

3.4 Circulation Distribution

3.4.1 Foil Circulation Distribution

For typical hydrofoil planforms at practical depths Prandtl's hypothesis, that each section of the wing acts as though it is an isolated section, and modified lift line theory adequately define the foil performance estimates and reduce those estimates to simple applications of the section characteristics, More detail than is usually provided with modified lift line discussions is required. Reference 1 is particularly well adapted to the hydrofoil case and the nomenclature of Reference 1 is employed here.

DeYoung's procedure is restricted to foils having straight quarter-chord lines on each semi-span. The number of control points is unrestricted but the systemizations of References l-4 employ seven control points on the span at the three-quarter chord station. The results are aerodynamic, i.e., infinite depth, and for a 2π section lift curve slope. The procedure can be performed as a desk calculation with considerable intuitive benefit or is adaptable to any level of automation. It is illustrated here in Section 3.4.1.1.

Reference 1 presents the foil basic and additional circulation distributions; Reference 2 presents flap circulation distribution, and Reference 3 presents the circulation distribution for antisymmetrical deflected flaps (ailerons). All three references are appropriate only for the inverted "T" configuration and no equivalent procedure for the inverted "π" configuration can be offered here. Reference 4 offers a basis for such a procedure but is far from ready for application.

Any procedure or computer program for circulation distribution which employs at least seven control points on the surface is adequate to the hydrofoil requirement. The seven point limitation is DeYoung's recommendation in Reference 1.

The circulation distribution is most conveniently considered in the non-dimensional form:

$$G = \frac{\Gamma}{bV} = \frac{c_\ell c}{2b} \qquad 3.4.1\text{-}1$$

where: Γ = circulation, m^2/s ($ft^2/sec.$), $\frac{c_\ell c V}{2}$

b = span, m (ft)

v = speed, m/s (ft/sec)

c_ℓ = section lift coefficient

c = section chord, M (ft)

A frequently employed alternative is derived from the form of Equation 3.4.1-1:

$$\frac{c_\ell c}{C_L c_{avg}} = \frac{2A}{c_{l_{\delta_1}}} \frac{G}{\delta_1} = \frac{G}{\delta_1} \Big/ \int_0^1 \frac{G}{\delta_1} d\eta \qquad 3.4.1\text{-}2$$

where: C_L = foil lift coefficient

C_{avg} = average foil chord, S/b

A = aspect ration, b^2/S

S = foil area

δ_1 = a general angle; pitch, incidence, full-chord flap, or flap angle.

REFERENCES

1. DeYoung, J. and C.W. Harper, "Theoretical Symmetric Span Loading At Subsonic Speeds For Wings Having Arbirtrary Plan Form," NACA Report 921, 1948.
2. DeYoung, J., "Theoretical Symmetric Span Loading Due to Flap Deflection for Wings of Arbitrary Plan Form at Subsonic Speeds," NACA Report 1071, 1952.
3. DeYoung, J., "Theoretical Antisymmetric Span Loading for Wings of Arbitrary Plan Form at Subsonic Speeds," NACA Report 1056 and NACA Technical Note 2140, 1950.
4. DeYoung, J., "Non-Planner Wing Load-Line and Slender Wing Theory," NASA Contractor Report 2864, 1977.

3.4.1.1 Additional Circulation Distribution - Tables 3.4.1.1-I and -II illustrate DeYoung's procedure by application to the AG(EH) main foil system and Figure 3.4.1.1-1 presents the results of those tables graphically. The AG(EH) planform was designed under aspect ratio and sweep constraints which are now obsolete but a substantial body of data is available for the foil in model and prototype scale and the planform provides a severe test of the application of Prandtl's hypothesis and modified lift line theory and of the incorporation of sweep into the cavitation characteristics.

Figure 3.4.1.1-1 introduces several definitions convenient to the subject.

"Pitch Lift" is that lift which results when the foil and pod(s) experience the same angle of attack and is designated $C_{L\alpha}$ on Figure 3.4.1.1-1. All lift is pitch lift when the foil/pod attachment is rigid. Craft and orbital motions produce pitch lift for any lift control system.

"Incidence Lift" is that lift produced by foil motion relative to the pod(s) and is designated C_{L_i} on Figure 3.4.1.1-1. At a rigid foil/pod intersection the incidence angle between the pod axis of symmetry and the foil chord plane produces an incidence lift component. Camber effectively increases that angle and produces an incidence lift component. Flap lift is incidence lift reduced by the value of the flap effectiveness. For a partial-exposed-span flap a second incidence lift curve would be added to Figure 3.4.1.1-1. Calculation of partial span flap circulation distributions is expedited by noting that circulation distributions are additive; e.g., the difference between the curves of Figure 3.4.1.1-1 is the circulation distribution for an inboard flap of 12.82% span.

The span has basic and additional lift distributions of definitions similar to those for the section chordwise lift distributions of Sections 3.3.2.1 and 3.3.2.3.

"Additional" foil circulation distribution is that circulation due to angle of attack. Both of the spanwise circulation distributions of Figure 3.4.1.1-1 are for additional lift.

"Basic foil" circulation is that circulation due to twist due to a spanwise mean lint twist distribution and/or a spanwise variation in section geometry. The basic circulation is that circulation which remains when the foil is set at the zero lift angle of attack. Basic circulation is discussed further in Section 3.4.1.2.

While the elliptic circulation distribution is an abstraction, all foil circulation distributions tend to be elliptic and particularly so for hydrofoils as illustrated on Figure 3.4.1.1-1. For an elliptic distribution most of the foil characteristics become explicit algebraic expressions and the elliptic distribution therefore providesan intuitive guide and numerical check for those characteristics. The elliptic distribution is given by:

$$\frac{G}{G_1} = \frac{G_{\eta=0}}{G_1}\sqrt{1-\eta^2} = \frac{\Gamma_0}{\pi A_1}\sqrt{1-\eta^2} \qquad 3.4.1.1\text{-}1$$

The lift curve slope is given by:

$$C_{L_{\alpha_1}} = 2A\int_0^1 \frac{G}{G_1}\,d\eta \qquad 3.4.1.1\text{-}2$$

This slope is aerodynamic (infinite depth) and for a 2 π section lift curve slope. For a flap it is for the full chord flap, d α /d β =1. Adjustments for section lift curve slope and flap effectiveness are incorporated in Section 3.5.

REFERENCES

1. DeYong, 3. and C.W. Harper, "Theoretical Symmetric Span Loading at Subsonic Speeds for Wings Having Arbitrary Plan Form," NACA Report 9.21, 1948.

2. DeYoung, J., "Theoretical Symmetric Span Loading Due to Flap Deflection for Wings of Arbitrary Plan Form at Subsonic Speeds," NACA Report 1071, 1952.

TABLE 3.4.1.1-I

PITCH LIFT CIRCULATION DISTRIBUTION

Note: Illustration is AG(EH) main foil system;
$A=3$, $\lambda=.3$, $\Lambda=35.2°$, $\eta_{pad}=.1282$

The circulation at four points on the semi-span is given by the solutions to the four equations:

$$a_{1n}\frac{G_1}{\delta_1}+a_{2n}\frac{G_2}{\delta_1}+a_{3n}\frac{G_3}{\delta_1}+a_{4n}\frac{G_4}{\delta_1}=\frac{\alpha_n}{\delta_1} \quad \text{for } n=1 \text{ to } 4$$

The influence coefficients, a_{rn}, are best obtained from Eq. (A37) of Ref. 1, which requires computer programming, but can be read from Fig. 1 of Ref. 1 or Ref. 2 for the parameter H_r:

TABLE 3.4.1.1-IA Wing Chord Distribution Parameter, H_r

r	η	d_r	$\frac{c_r}{c_{avg}}$	H_r
1	.92388	.061	.54351	.33670
2	.70711	.234	.77696	.90352
3	.38268	.381	1.1263	1.0148
4	0	.320	1.5385	.62398

$\eta=\cos\frac{r\pi}{8}$

d_r are constants given in Eq. 2 of Ref. 2

$$\frac{c_r}{c_{avg}}=\frac{2}{1+\lambda}\left[1-(1-\lambda)\eta_r\right]=\frac{1-.7\eta_r}{.65}$$

$$H_r=\frac{A\,d_r}{c_r/c_{avg}}=\frac{3\,d_r}{c_r/c_{avg}}$$

TABLE 3.4.1.1-IB Circulation Distribution Matrix, a_{rn}
AG(EH) Main Foil

r \ n	G_1/δ_1	G_2/δ_1	G_3/δ_1	G_4/δ_1	
	1	2	3	4	
1	10.8188	-3.6730	.088268	-.27362	$=\alpha_1/\delta_1$
2	-1.7711	6.0338	-2.3116	.057779	$=\alpha_2/\delta_1$
3	.094383	-1.5516	4.6163	-1.6503	$=\alpha_3/\delta_1$
4	-.16364	.18496	-2.8252	4.1710	$=\alpha_4/\delta_1$

TABLE 3.4.1.1-I (Cont.)

TABLE 3.4.1.1-IC Inverse Circulation Distribution Matrix

a_1/δ_1	a_2/δ_1	a_3/δ_1	a_4/δ_1		$\frac{G_n}{\delta_1} = \frac{G_n/\delta_1}{R_n}$
.10491	.076589	.052660	.026657	$= G_1/\delta_1 =$	.26082
.036198	.22363	.14626	.057147	$= G_2/\delta_1 =$	.46324
.014408	.093854	.34720	.13702	$= G_3/\delta_1 =$	.59248
.012270	.056659	.23075	.33107	$= G_4/\delta_1 =$	.63076

where $a_n/\delta_1 = 1$ for all n for pitch lift

Note: This matrix is the inverse of the matrix of Table 3.4.1.1-IB

Four interpolated points are available from Table A7 of Ref. 2. Note Erratum No. 1 correction for $C_{4,1/2}$.

TABLE 3.4.1.1-ID Interpolated Circulation Distribution

$\frac{G_1/\delta_1}{R_1}$	$\frac{G_2/\delta_1}{R_2}$	$\frac{G_3/\delta_1}{R_3}$	$\frac{G_4/\delta_1}{R_4}$		$\frac{G_K/\delta_1}{R_K} = \frac{G_K}{\delta_1}$
.8657	-.3753	.2778	-.1275	$= G_{1/2}/\delta_1 =$	.13611
.4904	.7682	-.3524	.1503	$= G_{3/2}/\delta_1 =$	.36978
-.0976	.5132	.7911	-.225	$= G_{5/2}/\delta_1 =$	.53907
.0229	-.0746	.4157	.641	$= G_{7/2}/\delta_1 =$	.62203

TABLE 3.4.1.1-I (Cont.)

TABLE 3.4.1.1-IE Pitch Lift Circulation Distribution

n or K	η	G_n/S_1 or G_K/S_1
4	0	.63076
7/2	.19509	.62203
3	.38268	.59248
5/2	.55557	.53907
2	.70711	.46324
3/2	.83147	.36978
1	.92388	.26082
1/2	.98079	.13611
0	1	0

From Tables 3.4.1.1-IC and -ID.

TABLE 3.4.1.1-II

INCIDENCE LIFT CIRCULATION DISTRIBUTION

Note: Illustration is AG(EH) main foil system;
$A = 3$, $\lambda = .3$, $\Lambda = 35.2°$, $\eta_{pod} = .1282$

TABLE 3.4.1.1-IIA Spanwise Loading For $A = 0$

n	SPAN STATION			$\left(\frac{G_n}{\delta_1}\right)_{A=0}$
	ϕ		η	
1	$\pi/8$	.39270	.92388	.34969
2	$\pi/4$	.78540	.70711	.63489
3	$3\pi/8$	1.1781	.38268	.79068
4	$\pi/2$	1.5708	0	.69438

$\phi = n\pi/8$ $\qquad$ $\theta = \cos^{-1}\eta_{pod} = 1.4423$

$\eta = \cos\phi$

From Eq. (A2), Ref. 2:

$$\left[\frac{G(\phi)}{\delta_1}\right]_{A=0} = \frac{1}{\pi}\left[2\theta\sin\phi + (\cos\phi - \cos\theta)\ln\left|\frac{\sin\frac{\theta+\phi}{2}}{\sin\frac{\theta-\phi}{2}}\right| + (\cos\phi + \cos\theta)\ln\left|\frac{\cos\frac{\theta+\phi}{2}}{\cos\frac{\theta-\phi}{2}}\right|\right]$$

TABLE 3.4.1.1-IIB Twist And Circulation Distribution; Eq. (A1), Ref. 2

n	$\left(\frac{G_1}{\delta_1}\right)_{A=0}$	$\left(\frac{G_2}{\delta_1}\right)_{A=0}$	$\left(\frac{G_3}{\delta_1}\right)_{A=0}$	$\left(\frac{G_4}{\delta_1}\right)_{A=0}$		$\frac{\alpha_n}{\delta_1}$	$\frac{G_n}{\delta_1}$
1	10.4524	-3.8284	0	-.2928	$= \alpha_1/\delta_1 =$	1.0212	.3
2	-2.0720	5.6568	-2.3888	0	$= \alpha_2/\delta_1 =$	.97811	.9
3	0	-1.8284	4.3296	-1.7022	$= \alpha_3/\delta_1 =$	1.0805	.5
4	-.2242	0	-3.1548	4	$= \alpha_4/\delta_1 =$	.20468	.6

For the $(G_n/\delta_1)_{A=0}$ of Table 3.4.1.1-IIA

$\frac{G_n}{\delta_1}$ is from inverse matrix of Table 3.4.1.1-IC

TABLE 3.4.1.1-II (Cont.)

TABLE 3.4.1.1-IIC Interpolation Parameter $\frac{G_n/\delta_1}{R_n}$

n	sin φ	$\left(\frac{G_n}{\delta_1}\right)_{A=0}$	R_n	$\frac{G_n}{\delta_1}$	$\frac{G_n/\delta_1}{R_n}$
1	.38268	.34969	.91379	.24441	.26747
2	.70711	.63489	.89787	.42543	.47382
3	.92388	.79068	.85583	.50971	.59558
4	1	.69438	.69438	.38504	.55451

$\sin \phi = \sin n\pi/8$

$(G_n/\delta_1)_{A=0}$ from Table 3.4.1.1-IIA

$R_n = (G_n/\delta_1)_{A=0} / \sin \phi$

G_n/δ_1 from Table 3.4.1.1-IIB

TABLE 3.4.1.1-II D Interpolated Circulation Distribution

K	$\frac{G_K/\delta_1}{R_K}$	Φ		η	sin φ	$\left(\frac{G_K}{\delta_1}\right)_{A=0}$	R_K	$\frac{G_K}{\delta_1}$
1/2	.14848	π/16	.19635	.98079	.19509	.17892	.91712	.13617
3/2	.36862	3π/16	.58905	.83147	.55557	.50429	.90770	.33460
5/2	.56346	5π/16	.98175	.55557	.83147	.73354	.88222	.49710
7/2	.57380	7π/16	1.37445	.19509	.98079	.78498	.80035	.45924

$\frac{G_K/\delta_1}{R_K}$ is from $\frac{G_n/\delta_1}{R_n}$ from Table 3.4.1.1-IIC in matrix of Table 3.4.1.1-ID

$\phi = K\pi/8$

$\eta = \cos \phi$

$\left(\frac{G_K}{\delta_1}\right)_{A=0}$ is from equation shown under Table 3.4.1.1-IIA

$R_K = (G_K/\delta_1)_{A=0} / \sin \phi$

$\frac{G_K}{\delta_1} = \frac{G_K/\delta_1}{R_K} \times R_K$

TABLE 3.4.1.1-II (Cont.)

TABLE 3.4.1.1-IIE Incidence Lift Circulation Distribution

n or K	η	G_n/δ_1 or G_K/δ_1
4	0	.38504
7/2	.19509	.45924
3	.38268	.50971
5/2	.55557	.49710
2	.70711	.42543
3/2	.83147	.33460
1	.92388	.24441
1/2	.98079	.13617
0	1	0

From Tables 3.4.1.1-IIB and -IID

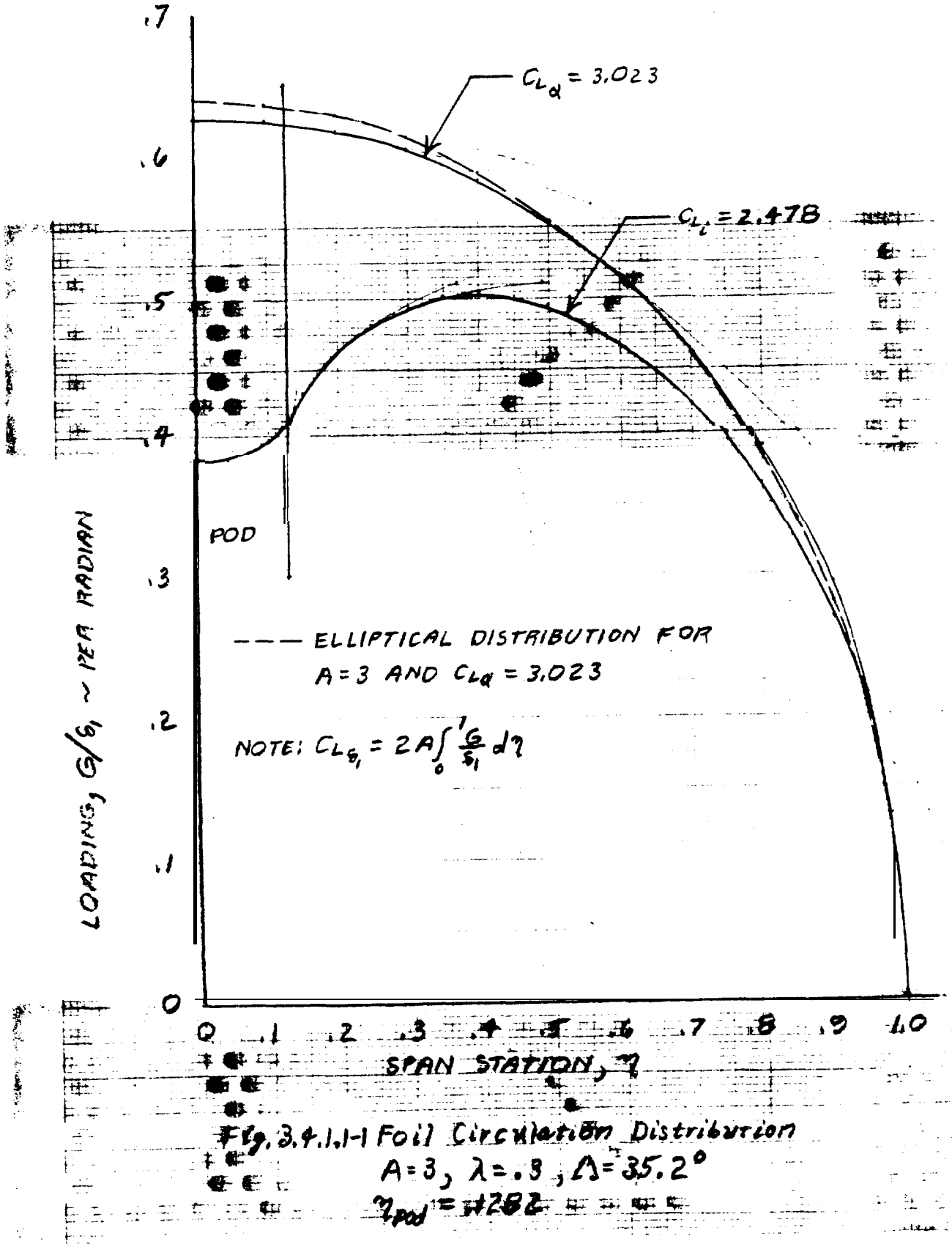

Fig. 3.4.1.1-1 Foil Circulation Distribution
$A = 3$, $\lambda = .3$, $\Lambda = 35.2°$
$\eta_{pod} = .282$

HAW 8/26/82

3.4.1.2 Basic Circulation Distribution - The foil may be twisted by twisting the mean line or by varying the section geometry, usually the camber, along the span. The twist produces a basic, or zero lift, circulation distribution which is added to the additional circulation for any angle of attack. The derivation of the basic lift distribution is not illustrated here. The procedure is included in Reference 1 and in several numerical procedures.

Twist is usually suggested as a means for improving the cavitation bucket and that application is illustrated on Figures 3.4.1.2-1 and -2 where a highly idealized twist is employed to produce a uniform section lift coefficient at a .2 foil lift coefficient. The incipient cavitation bucket advantage is quite small for the upper surface boundaries and the effective boundary may be closer to the incipient boundary for a uniform spanwise lift coefficient distribution; such a design should be examined closely in model scale before adoption. Foil twist might also be employed for wake adaptation.

There is a significant reservation with regard to the application of twist. It adds substantial complexities and uncertainties, which cannot be resolved with confidence in model scale, to the estimation of all of the foil characteristics and it is an irreversible design feature. Effective twist can be achieved equally well for all practical purposes by the use of simulated flaps in the form of trailing edge wedges which can be readily installed and modified on the prototype. Secondary controls for the control of the cavitation bucket are discussed in Section 3.8.

Foil structural flexibility produces a twist which can be accounted for by the addition of a basic circulation distribution. For solid foils of typical planform, sweep less than 15° and aspect ratio less than 6, the twist due to load is negligible.

REFERENCES

1. DeYoung, J. and C.W. Harper, "Theoretical Symmetric Span Loading at Subsonic Speeds for Wings Having Arbitrary Plan Form," NACA Report 921, 1948.

FIG. 3.4.1.2-1

FOIL TWIST

FOR UNIFORM SPANWISE c_l DISTRIBUTION

AT $C_L = .168$

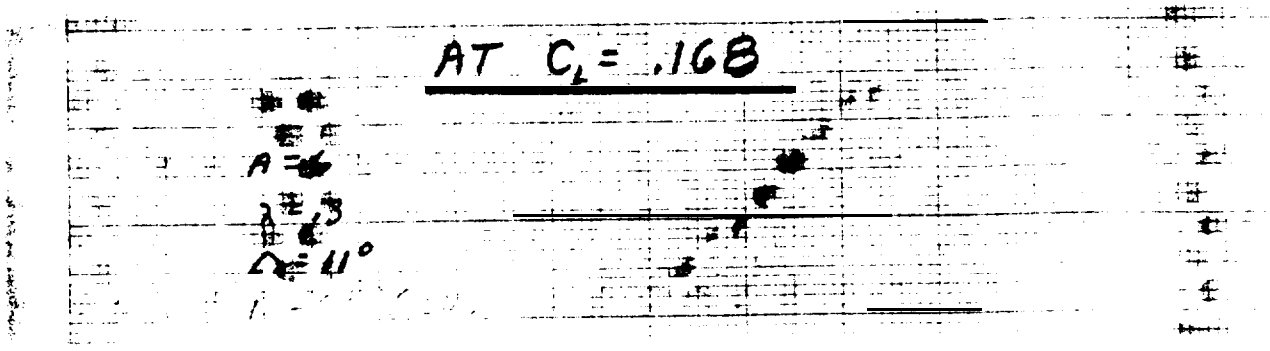

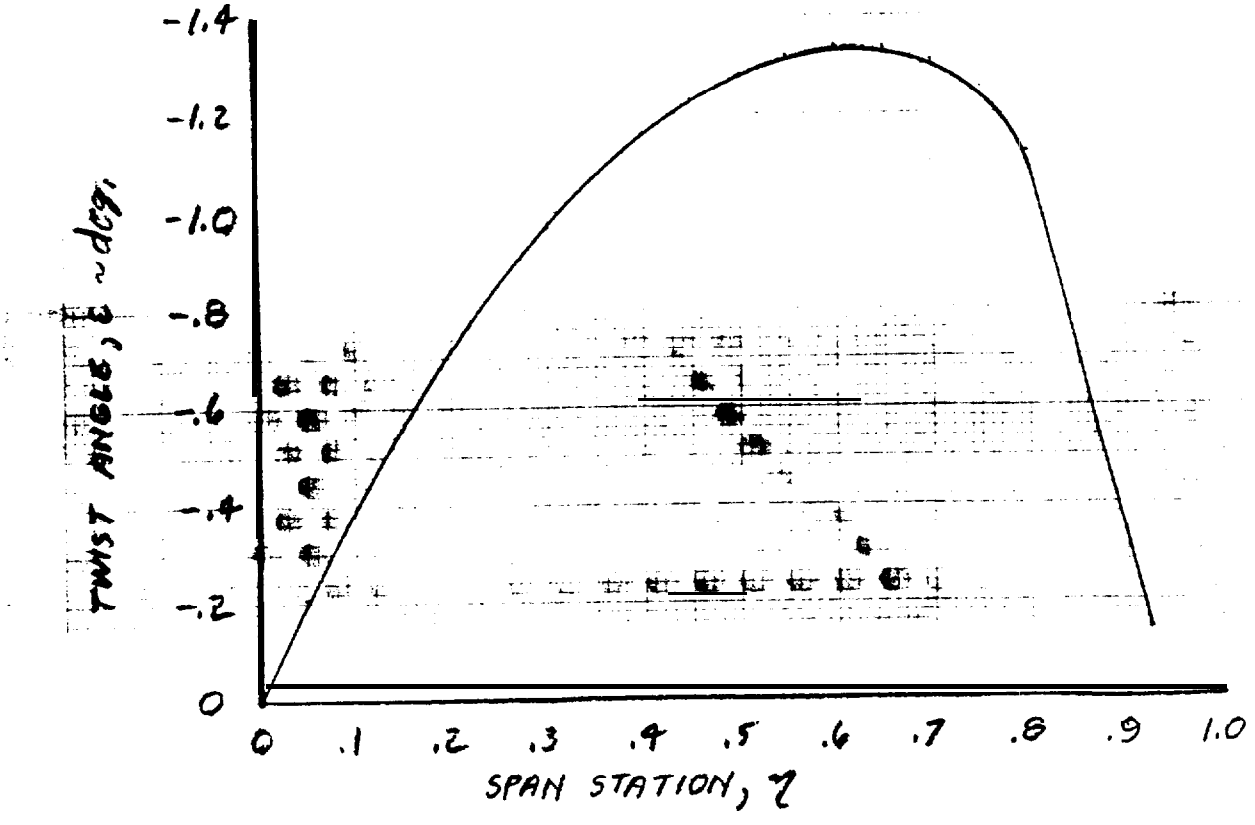

HAW 11/18/83 (M-88-10)

FIG. 3.4.1.2-2

LIFT DISTRIBUTION FOR TWISTED FOIL

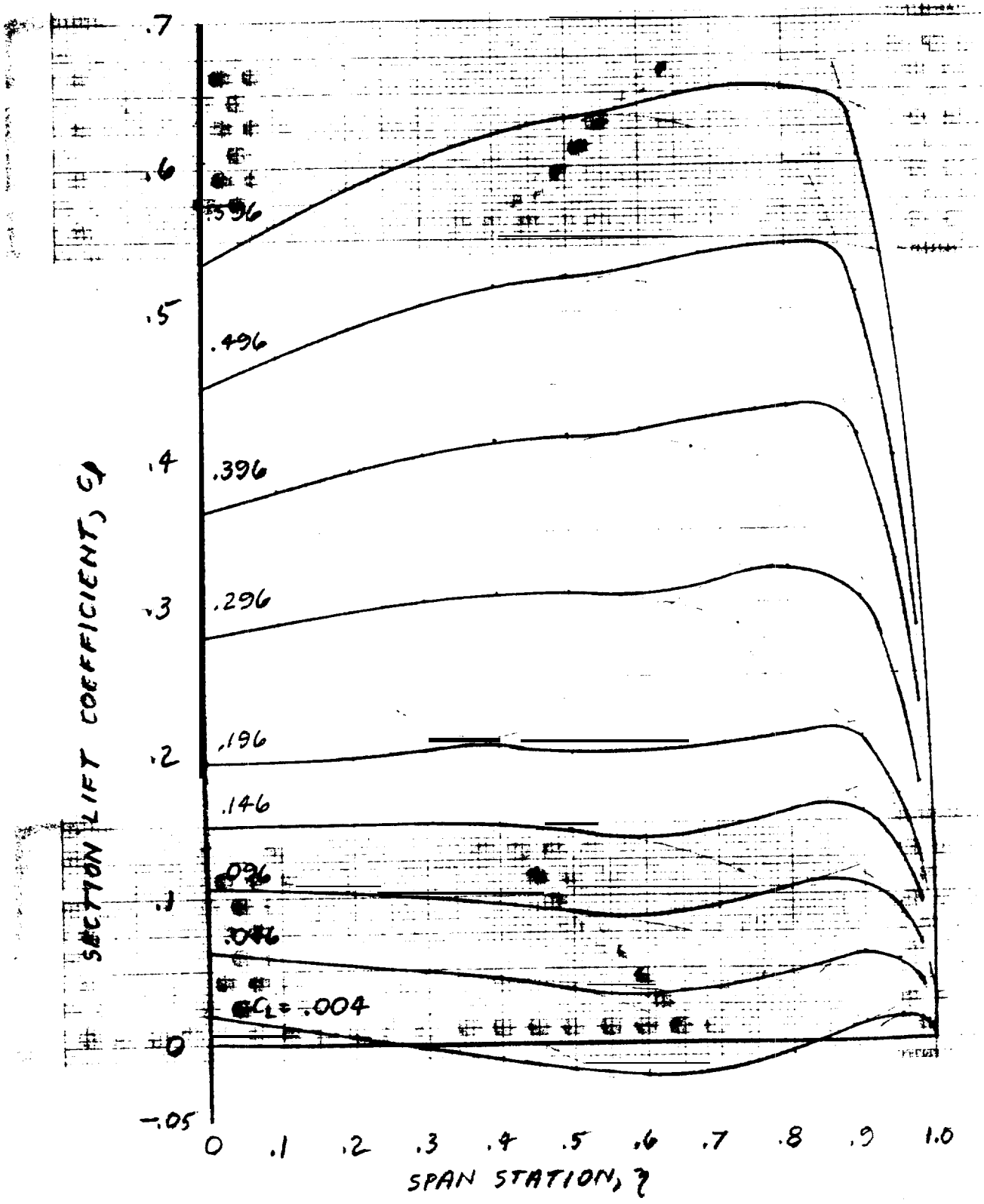

HRW 11/21/83 (M-88-10)

3.4.1.3 Antisymmetric Circulation Distribution - The practical hydrodynamic case presents antisymmetrically deflected flaps on an inverted " π " configuration and no procedure accounting for the strut influence can be offered here. Reference 1 is well systematized for the inverted "T" configuration but that configuration does not offer adequate rolling moment in a practical aspect ratio.

This characteristic is required to establish the cavitation limitations on the rolling moment as well as for the rolling moment itself.

REFERENCES

1. DeYoung, J., "Theoretical Antisymmetric Span Loading for Wings of Arbitrary Plan Form at Subsonic Speeds," NACA Report 1056 and NACA Technical Note 2140, 1950.

3.4.2 Foil Loading Distribution

3.4.2.1 Lift Coefficient Distribution

The spanwise distribution for the section lift coefficient is given by:

$$\frac{c_l}{c_i} = \frac{2A}{c_{l_\alpha}\delta_1}\,\frac{c_{avg}}{c}\,\frac{G}{\delta_1} \qquad \text{3.4.2.1-1}$$

where: $c_{l_{\alpha_1}}$ is the lift curve slope of Equation 3.4.1.1-2

G/δ_1 is the circulation distribution of 3.4.1-1

For the elliptical circulation distribution on a semi-span of straight leading and trailing edge Equation 3.4.2.1-1 becomes:

$$\frac{c_l}{c_i} = \frac{2A}{c_{l_\alpha}} \times \frac{1+\lambda}{2}\left[1-(1-\lambda)\eta\right]^{-1} \times \frac{2c_{l_\alpha}}{\pi A}\sqrt{1-\eta^2} \qquad \text{3.4.2.1-1}$$

$$= \frac{2}{\pi}(1+\lambda)\frac{\sqrt{1-\eta^2}}{1-(1-\lambda)\eta}$$

$$\left(\frac{c_l}{c_i}\right)_{max} = \frac{2}{\pi}\frac{1+\lambda}{\sqrt{1-(1-\lambda)^2}} \quad \text{at } \eta = 1-\lambda$$

Equations 3.4.2.1-1 and-2 are illustrated on Figure 3.4.2.1-l. Upper surface cavitation will appear first at that span station having maximum section lift coefficient; lower surface cavitation will appear first at that inboard station having minimum section lift coefficient - the tip vortex core is normally cavitated in flight. As the cavitation spreads on the chord and span it effectively twists the foil and invalidates the theoretical distribution for lift coefficients outside of the wetted range.

Schrenk's method for estimating spanwise lift distribution, e.g. as presented by Pope in Reference 2, provides a result similar to Equation 3.4.2.1-2 which is compared with that equation and with certain results out of Reference 1 on Figure 3.4.2.1-z.

REFERENCES

1. DeYoung, J. and C.W. Harper, "Theoretical Symmetric Span Loading at Subsonic Speeds for Wings Having Arbitrary Plan Form," NACA Report 921, 1948.

2. Pope, A., "Basic Wing and Airfoil Theory," McGraw-Hill, 1951.

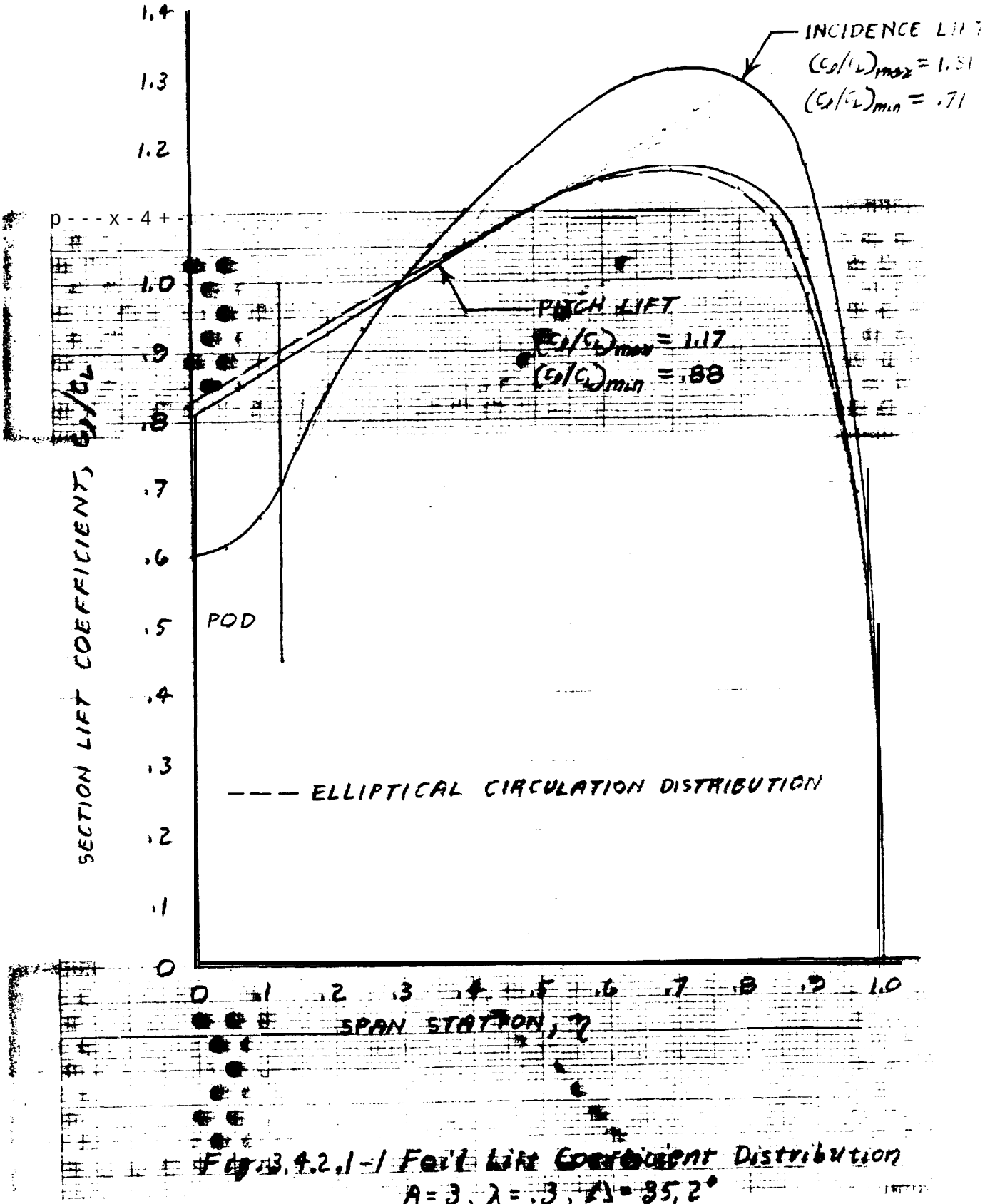

Fig. 3.4.2.1-1 Foil Lift Coefficient Distribution
$A = 3, \lambda = .3, \Lambda = 35.2°$
$\eta_{pod} = .1282$

HRW 8/27/82

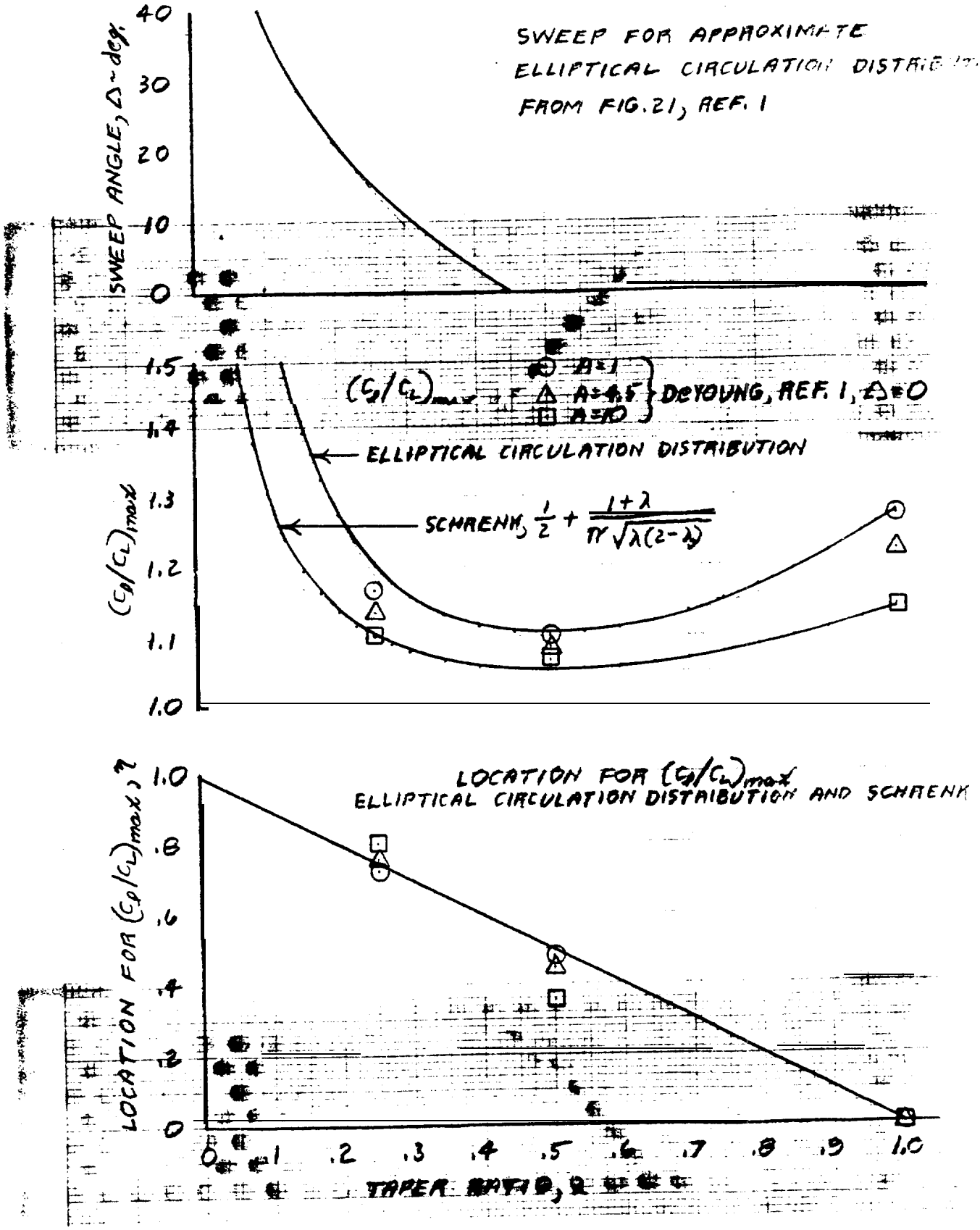

Fig. 3.4.2.1-2 Planform Design Considerations

HRW 8/27/82

3.4.2.2 Shear Distribution

The first integral of the circulation distribution is the foil shear distribution which has unit value for the full semi-span:

$$\frac{V}{L'/2} = \frac{2A}{c_2 s_1} \int_{\eta}^{1} \frac{G}{s_1} d\eta \qquad \text{3.4.2.2-1}$$

where L' = the foil-only lift, i.e., without the pod lift increment of Section 3.5.1

Integrated over the exposed semi-span this integral provides the lift carried on the incidence hinge when the incidence motion is at the foil/pod intersection.

For the elliptical circulation distribution of Equation 3.4.1.1-1 the shear distribution becomes:

$$\frac{V}{L'/2} = 1 - \frac{2}{\pi}\left(\eta\sqrt{1-\eta^2} + \sin^{-1}\eta\right) \qquad \text{3.4.2.2-2}$$

Equations 3.4.2.2-1 and -2 are illustrated on Figure 3.4.2.2-1 for the circulation distributions of Figure 3.4.1.1-1.

It is important to note that this volume is limited to consideration of effectively wetted foil performance, i.e., performance within the effective cavitation boundary. Thus normal control loads, including most of the load range signficant to fatigue, are presented. However, the effective foil twist associated with advanced cavitation and important to limit foil loads is not considered here and, in general, the load distribution discussion and development here is not directed to structural design.

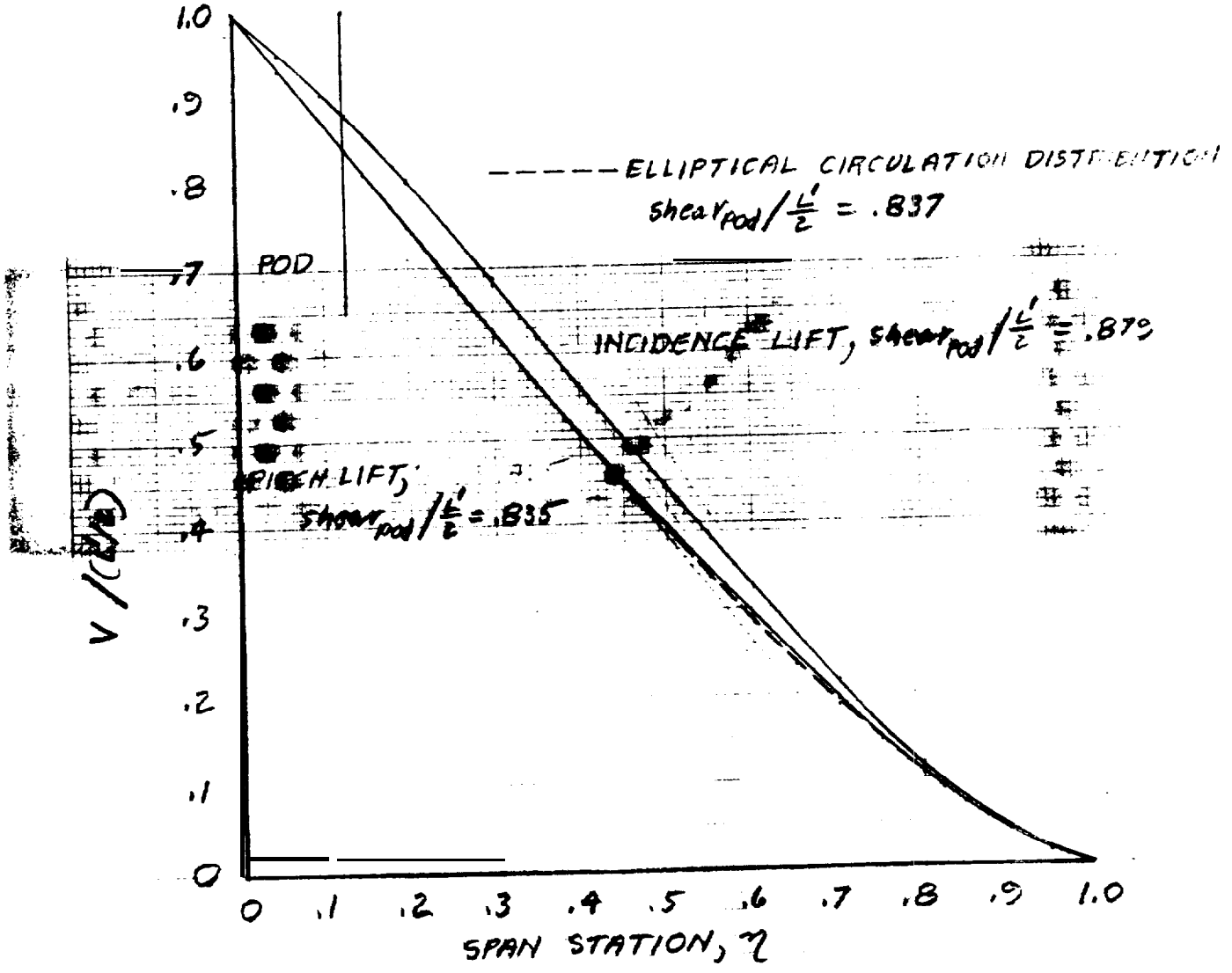

Fig. 3.4.2.2-1 Foil Shear Distribution
$A = 3$, $\lambda = .3$, $\Lambda = 35.2°$
$\eta_{pod} = .128$

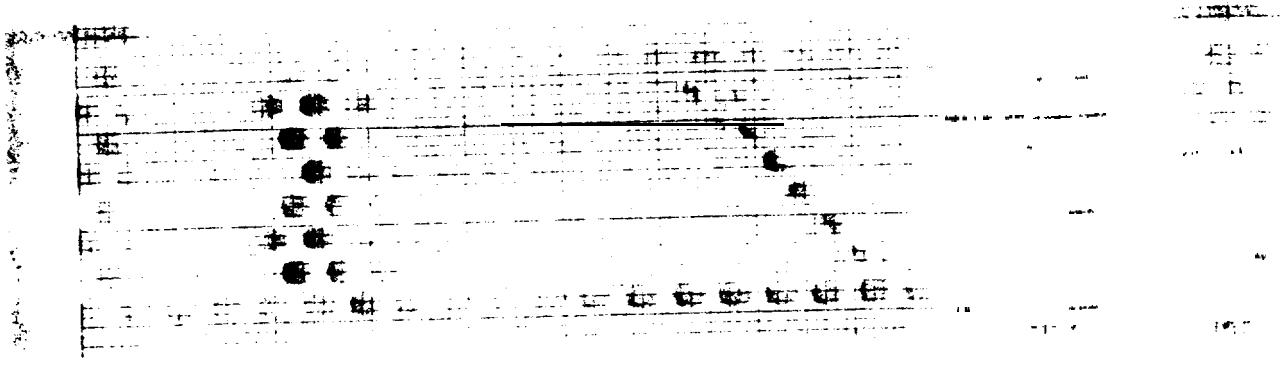

HFW 8/34/82

3.4.2.3 Bending Moment Distribution - The non-dimensional moment distribution is the integral of the non-dimensional shear distribution:

$$\frac{M_\eta}{\frac{L'}{2}\frac{b}{2}} = \frac{V_\eta}{L'/2}\,\eta_{c.p._\eta} = \int_\eta^1 \frac{V}{L'/2}\,d\eta = \frac{2A}{c_l \delta_1}\int_\eta^1\int_\eta^1 \frac{G}{\delta_1}\,d\eta\,d\eta \qquad 3.4.2.3\text{-}1$$

where $\eta_{c.p._\eta}$ = the moment arm expressed as a fraction of the semi-span

$= \eta_{c.p._1} - \eta$

Integrated from pod to tip Equation 3.4.2.3-l locates the center of pressure for that portion of the additional load carried on the exposed foil:

$$\frac{M_{pod}}{\frac{L'}{2}\frac{b}{2}} = \frac{V_{pod}}{L'/2}\,\eta_{c.p._{pod}} = \frac{V_{pod}}{L'/2}\left(\eta_{c.p._1} - \eta_{pod}\right)$$

$$= \int_{\eta_{pod}}^1 \frac{V}{L'/2}\,d\eta = \frac{2A}{c_l \delta_1}\int_{\eta_{pod}}^1\int_\eta^1 \frac{G}{\delta_1}\,d\eta\,d\eta \qquad 3.4.2.3\text{-}2$$

Extended over the entire semi-span the integral **becomes the** spanwise location for the additional load center of pressure:

$$\eta_{c.p._1} = \int_0^1 \frac{V}{L'/2}\,d\eta = \frac{2A}{c_l \delta_1}\int_0^1\int_\eta^1 \frac{G}{\delta_1}\,d\eta\,d\eta \qquad 3.4.2.3\text{-}3$$

For the partial-exposed-span flap the integral is required over the spanwise **extent of the flap.**

In general the center of pressure for the loading over any portion of the span is given by:

$$\eta_{c.p.} = \eta + \frac{M_\eta}{\frac{L'}{2}\frac{b}{2}} \Big/ \frac{V_\eta}{L'/2}$$

$$= \frac{M}{\frac{L'}{2}\frac{b}{2}} \Big/ \frac{V}{L'/2} \qquad \text{for entire semi-span.} \qquad 3.4.2.3\text{-}4$$

For the elliptical circulation shear distribution of Equation 3.4.2.2-Z **the moment distribution becomes:**

$$\frac{M_\eta}{\frac{L'}{2}\frac{b}{2}} = \frac{2}{\pi}\left[\frac{\eta^2+2}{3}\sqrt{1-\eta^2} + \eta\left(\sin^{-1}\eta - \frac{\pi}{2}\right)\right] \qquad 3.4.2.3\text{-}5$$

$$\eta_{c.p._1} = 4/3\pi$$

The moment distributions are illustrated on Figure 3.4.2.3-I.

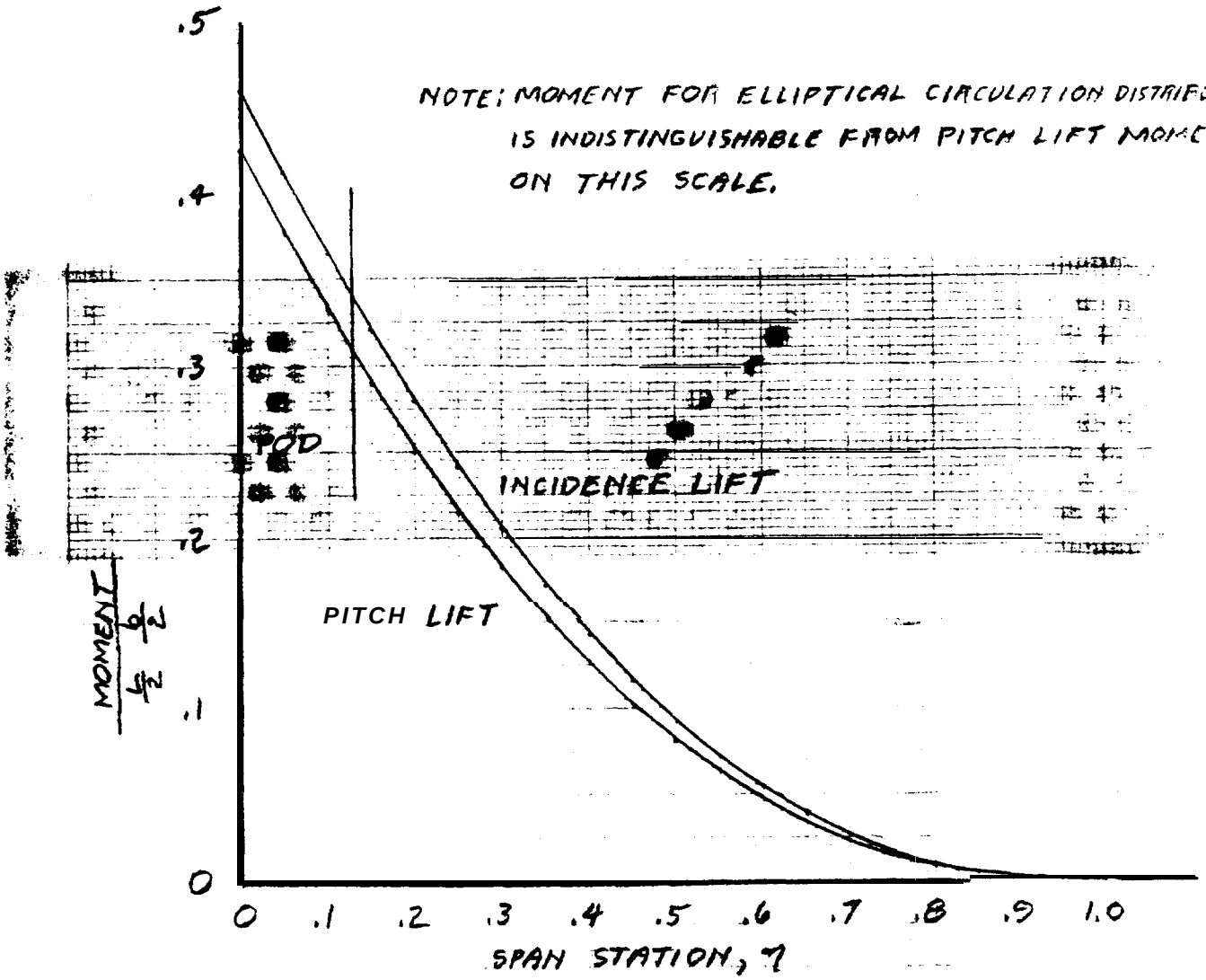

CIRCULATION DISTRIBUTION	FOIL AREA	SHEAR / (L/2)	MOMENT / (L/2)(b/2)	$\eta_{C.P.}$
ELLIPTICAL	TOTAL	1	.424	.424
	EXPOSED	.837	.307	.494
PITCH LIFT	TOTAL	1	.426	.426
	EXPOSED	.835	.309	.438
INCIDENCE LIFT	TOTAL	1	.460	.460
	EXPOSED	.879	.339	.514

Fig. 3.4.2.3-1 Foil Moment Distribution

$A = 3$, $\lambda = .3$, $\Lambda = 35.2°$

$\eta_{pod} = .1282$

HRW 8/31/82

3.4.3 Foil Aerodynamic Centers

In aerodynamic practice the aerodynamic center is significant only to craft trim and the wing "aerodynamic center" is the pitch lift aerodynamic center, expressed as a fraction of the mean aerodynamic chord. The hydrodynamic case adds complexities requiring a well systematized view of the foil pitching moments.

In particular, for the hydrodynamic case it is more convenient to locate the foil aerodynamic centers and the flap center of pressure on the chord at the foil plane of symmetry and express them as fractions of that chord. The chord at the foil plane of symmetry is referred to here as the foil root chord, which is not to be confused with the chord at the foil/pod intersection.

For a semi-span of straight leading and trailing edges, the following equation expresses a station on the chord at span station as a fraction of the root chord:

$$\frac{x}{c_r} = \left[1-(1-\lambda)\eta\right]\frac{x}{c} + \frac{1}{4}\left[1-\lambda+A(1+\lambda)\tan\Lambda\right]\eta \qquad 3.4.3\text{-}1$$

Equation 3.4.3-l is employed throughout the following sections but it must be noted that appropriate modifications are required if the semi-spans do not have straight leading and trailing edges.

3.4.3.1 Craft Trim Aerodynamic Centers - The foil aerodynamic center for pitch and incidence lift is the aerodynamic center for the section at the spanwise center of pressure. Then by reference to Equation 3.4.3-l:

$$a.c._\alpha \equiv \left[1-(1-\lambda)\eta_{c.p._\alpha}\right]a.c. + \frac{1}{4}\left[1-\lambda+A(1+\lambda)\tan\Lambda\right]\eta_{c.p._\alpha} \qquad 3.4.3.1\text{-}1$$

$$a.c._i \equiv \left[1-(1-\lambda)\eta_{c.p._i}\right]_{a.c.} + \frac{1}{4}\left[1-\lambda+A(1+\lambda)\tan\Lambda\right]\eta_{c.p._i} \qquad 3.4.3.1\text{-}2$$

where: $a.c._\alpha$, $a.c._i$ = pitch and incidence lift aerodynamic centers expressed as fraction of root chord

$\eta_{c.p._\alpha}$, $\eta_{c.p._i}$ = pitch and incidence lift spanwise centers of pressure from Equation 3.4.2.3-4

$a.c._\ell$ = section aerodynamic center from Figure 3.3.2.1-10

λ = taper ratio, c_t/c_r

c_t = tip chord

c_r = root chord, chord at foil plane of symmetry

A = aspect ratio, b^2/S

b = foil span

S = foil area

Λ = quarter-chord line sweep

Referring to Section 3.3.3.2, the center of pressure for the section flap lift is given by:

$$c.p._F = a.c._\ell + \zeta(c.p._\beta - a.c._\ell)$$
$$= a.c._\ell + \zeta\left(\frac{1}{4} + \frac{1}{2}\frac{h}{c} - a.c._\ell\right) \qquad 3.4.3.1\text{-}3$$

The $\frac{1}{4}$ coefficient is the thin airfoil inviscid aerodynamic center and it would be just as accurate, perhaps more so, to identify this with the experimental a.c. to write Equation 3.4.3.1-3 as:

$$c.p._F = a.c._\ell + \frac{1}{2}\zeta\frac{h}{c} \qquad 3.4.3.1\text{-}4$$

where: a.c. = section aerodynamic center from Figure 3.3.2.1-10

ζ = Flap lift distribution parameter from Figure 3.3.2.4-l

h/c = hinge station expressed as fraction of chord

Then by reference to Equation 3.4.3-1, the flap lift center of pressure is located on the root chord at:

$$c.p._\zeta = \left[1-(1-\lambda)\eta_{c.p._\beta}\right]c.p._F + \frac{1}{4}\left[1-\lambda+A(1+\lambda)\tan\Lambda\right]\eta_{c.p._\beta} \qquad 3.4.3.1\text{-}5$$

where: $\eta_{c.p._\delta}$ = flap lift spanwise center of pressure from Equation 3.4.2.3-4

$c.p._F$ = center of pressure for section flap lift from Equation 3.4.3.1-4

3.4.3.2 Incidence Moment Aerodynamic centers - If the foil/pod intersection is rigid the trim aerodynamic centers are the incidence moment aerodynamic centers. If the pod/strut intersection is rigid the shear and moment integrals of Equation 3.4.2.3-4 extend only over the exposed foil. Equations 3.4.3.1-1, -2, and -5 are identical except for the spanwise centers of pressure:

$$a.c._{\alpha_i} \equiv \left[1-(1-\lambda)\eta_{c.p._{\alpha_i}}\right] a.c._\circ + \frac{1}{4}\left[1-\lambda+A(1+\lambda)\tan\Lambda\right]\eta_{c.p._{\alpha_i}} \qquad 3.4.3.2\text{-}1$$

$$a.c._{i_i} \equiv \left[1-(1-\lambda)\eta_{c.p._{i_i}}\right] a.c._\circ + \frac{1}{4}\left[1-\lambda+A(1+\lambda)\tan\Lambda\right]\eta_{c.p._{i_i}} \qquad 3.4.3.2\text{-}2$$

$$c.p._{\delta_i} \equiv \left[1-(1-\lambda)\eta_{c.p._{\delta_i}}\right] c.p._F + \frac{1}{4}\left[1-\lambda+A(1+\lambda)\tan\Lambda\right]\eta_{c.p._{\delta_i}} \qquad 3.4.3.2\text{-}3$$

3.4.3.3 Flap Moment Aerodynamic Centers - For semi-spans of straight leading and trailing edges and constant flap chord ratios, the flap hinge moment calculations are simplified by defining aerodynamic centers where the integration extends only over the flapped span:

$$a.c._{\alpha_\delta} \equiv \left[1-(1-\lambda)\eta_{c.p._{\alpha_\delta}}\right] a.c._\circ + \frac{1}{4}\left[1-\lambda+A(1+\lambda)\tan\Lambda\right]\eta_{c.p._{\alpha_\delta}} \qquad 3.4.3.3\text{-}1$$

$$a.c._{i_\delta} \equiv \left[1-(1-\lambda)\eta_{c.p._{i_\delta}}\right] a.c._\circ + \frac{1}{4}\left[1-\lambda+A(1+\lambda)\tan\Lambda\right]\eta_{c.p._{i_\delta}} \qquad 3.4.3.3\text{-}2$$

$$c.p._{\delta_\delta} \equiv \left[1-(1-\lambda)\eta_{c.p._{\delta_{\delta\delta}}}\right] c.p._F + \frac{1}{4}\left[1-\lambda+A(1+\lambda)\tan\Lambda\right]\eta_{c.p._{\delta_\delta}} \qquad 3.4.3.3\text{-}3$$

3.4.3.4 Foil Aerodynamic Center Summary - The general case presents the six aerodynamic centers and three flap lift centers of pressure of Table 3.4.3.4-I.

The nominal aerodynamic center uncertainty range of Table 3.4.3.4-I is from Figure 13 of Reference 1.

REFERENCES

1. DeYoung, J. and C.W. Harper, "Theoretical Symmetric Span Loading at Subsonic Speeds for Wings Having Arbitrary Plan Form," NACA Report 921, 1948.

TABLE 3.4.3.4-I

AERODYNAMIC CENTER PARAMETERS

	SYMBOL	INTEGRATION RANGE INBD	INTEGRATION RANGE OUTBD	CIRCULATION DISTRIBUTION	NOTE
CRAFT TRIM AND FIXED FOIL/POD INCIDENCE LIFT CONTROL	$a.c._\alpha$	FULL SEMI-SPAN		G/α	
	$a.c._{i'}$			G/i'	
	$c.p._\delta$			G/δ	FLAP LIFT CONTROL SYSTEMS ONLY
INCIDENCE LIFT CONTROL WITH FOIL/POD MOTION	$a.c._{\alpha_i}$	POD	TIP	G/α	INCIDENCE LIFT CONTROL SYSTEMS ONLY
	$a.c._{i_i}$			G/i	
	$c.p._{\delta_i}$			G/δ	INCIDENCE + FLAP LIFT CONTROL SYSTEMS ONLY.
FLAP LIFT CONTROL	$a.c._{\alpha_\delta}$	FLAPPED SPAN EXTREMITIES		G/α	FLAP LIFT CONTROL SYSTEMS ONLY
	$a.c._{i'_\delta}$			G/i'	
	$c.p._{\delta_\delta}$			G/δ	

Note: Nominal aerodynamic center uncertainty is +5%, -1% of MAC

3.4.4 Strut Circulation Distribution and Side Force

Kochin shows in Reference 4 that when a vortex line moves transversely beneath a free surface at a Froude Number of 2 or more, the free surface can be represented by a biplane image of the vortex line. It follows that the free surface appears to be a biplane image for the bound vortex associated with a hydrofoil and, if the image vortex system is to be continuous, for the free vortex associated with the hydrofoil. Thus Kochin's result is extended to the entire hydrofoil vortex system in References 5 and 6 and throughout the literature.

For the strut the biplane image of the free vortex presents the strut as one semi-span of a foil having antisymmetrically deflected full-span, full-chord flaps and this is the model presented in Reference 5 and approximately as one option, continuous circulation, on Figure 32 of Reference 1. In fact Kochin's analysis shows that at rest a vortex line free surface image is a mirror image which presents the strut simply as one semi-span of a foil and this is the model of References 7 and 8.

The circulation distributions for these two models are compared on Figure 3.4.4-l which was taken from Figure 3 of Reference 2 for the mirror image and derived from Reference 3 for the biplane image. The side force slope variations with aspect ratio for the two models are compared on Figure 3.4.4-2 which was taken from Reference 3 and from Figure 4 of Reference 2. Note that the water line distortions on the strut are not accounted for on Figure 3.4.4-l and are most significant to the mirror image model. References 9 and 10 simply consider the wetted strut a foil, and lie between the two curves of Figure 3.4.4-2 along with several approximate equations for all three models which appear in the literature.

All of the measured strut side force slopes found were for 12% thick sections and the data of Reference I is typical. Strut side force curves are so distorted that slope measurements are judgemental and the Reference 1 slopes of Figure 3.4.4-2 are somewhat lower than those of Figure 32 of Reference 1 to discount an initial cavitation effect which increases slopes. By either interpretation the Reference 1 data and similar Grumman whirling tank data would seem to validate the biplane image.

Thickness ratios of 6% to 15% were tested in the whirling tank experiment with the result shown on Figure 3.4.4-3. The data of Figure 3.4.4-3 has been corrected for the section slope of Table 3.3.1.2-XI and for the Reynolds Number effect of Equation 3.3.1.1-1 to make the results directly comparable with DeYoung's slopes of Figure 3.4.4-2. The thickness effect of Figure 3.4.4-3 has not been seen in the literature and is of unknown origin. When that thickness effect is eliminated by extrapolation to zero thickness,, the zero thickness comparison of Figure 3.4.4-2 is obtained. The surface distortion effect, which would be most significant at low aspect ratio, remains unaccounted for.

Evidently there does not yet exist a confident prediction for the side force for the plain, rectangular, constant section strut and this important characteristic must be measured in model scale for the foil/pod/strut configuration. Reference 5 provides an estimate for the side force slope which is adequate for preliminary purposes:

$$C_{Y_\beta} \equiv \frac{Y}{q S_s \beta} = \frac{2\pi A}{AE + K_s K_E} + \frac{S}{S_s} C_{L_\alpha} \sin^2 \Gamma \qquad 3.4.4\text{-}1$$

where: Y = side force

β = sideslip angle

q = dynamic pressure, $\rho V^2/2$

S_s = wetted strut area, $h\, c_{avg}$

h = foil depth

c_{avg} = average chord for strut leading and trailing edge extended to foil plane

A = strut aspect ratio, h/c_{avg}

E = emperical factor $\approx 1 + \frac{1}{A}$

K_S = emperical factor $\approx$ 2.12

K_E = $\frac{1+b/h}{1+2b/h}$

b = foil span

S = foil area

C_{L_α} = foil pitch lift curve slope

Γ = foil dihedral angle

The emperical constants, E and K_S, can be adjusted as required to define the measured slopes when obtained. The side force should be measured while measuring the closure angle, Section 3.9, and the measurements should be extended to the ventilation angle for positive and negative yaw. The slope of Equation 3.4.4-1 will generally be limited to a short linear segment in the vicinity of zero yaw.

The strut side force can be considered uniformly distributed on the strut quarter-chord line.

REFERENCES

1. Rothblum, R.S., D.A. Mayer, and G.M. Wilburn, "Ventilation, Cavitation and Other Characteristics of High Speed Surface-Piercing Struts," NSRDC Report 3023, July 1969.
2. DeYoung, J. and C.W. Harper, "Theoretical Symmetric Span Loading at Subsonic Speeds for Wings Having Arbitrary Plan Form," NACA Report 921, 1948.
3. DeYoung, J., "Theoretical Antisymmetric Span Loading for Wings of Arbitrary Plan Form at Subsonic Speeds," NACA Report 1056 and NACA Technical Note 2140, 1950.
4. Kochin, N.E., I.A. Kibel, and N.V. Roze, "Theoretical Hydromechanics," Interscience Publishers, John Wiley & Sons, 1964.
5. Michel, W.H. et al, "Hydrofoil Handbook Vol. II, Hydrodynamic Characteristics of Components," Bath Iron Works Corp. by Gibbs and Cox, Inc., 1954.
6. Wadlin, Shuford, and McGehee, "A Theoretical and Experimental Investigation of the Lift and Drag Characteristics of Hydrofoils at Subcritical and Super Critical Speeds," NACA Report 1232, 1955.
7. "Hydrodynamic Characteristics of Base-Vented and Supercavitating Struts for Hydrofoil Ships," Vol. I-Text and Appendices, Aerojet Report No. 2796, August 1964.
8. Mostow, G., "On The Lateral Stability of a Hydrofoil Craft; Circulation Distribution Along a Surface Piercing Strut," Hydrofoil Corporation Technical Report HA-7, November 1952.

9. Wetzel J., "Experimental Studies of Air Ventilation of Vertical, Semi-Submerged Bodies," University of Minnesota Project Report No. 57, July 1957.

10. Rowe and Scherer, "Experimental Determination of the Static and Dynamic Coefficients of Surface-Piercing Struts," Hydronautics Technical Report 809-1, Feb. 1970.

FIG. 3.4.4-1

STRUT CIRCULATION DISTRIBUTION

RECTANGULAR STRUT

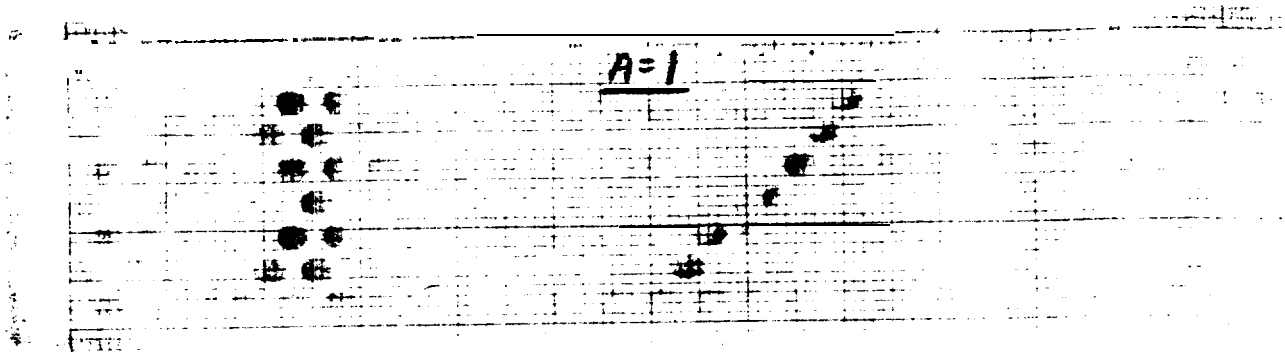

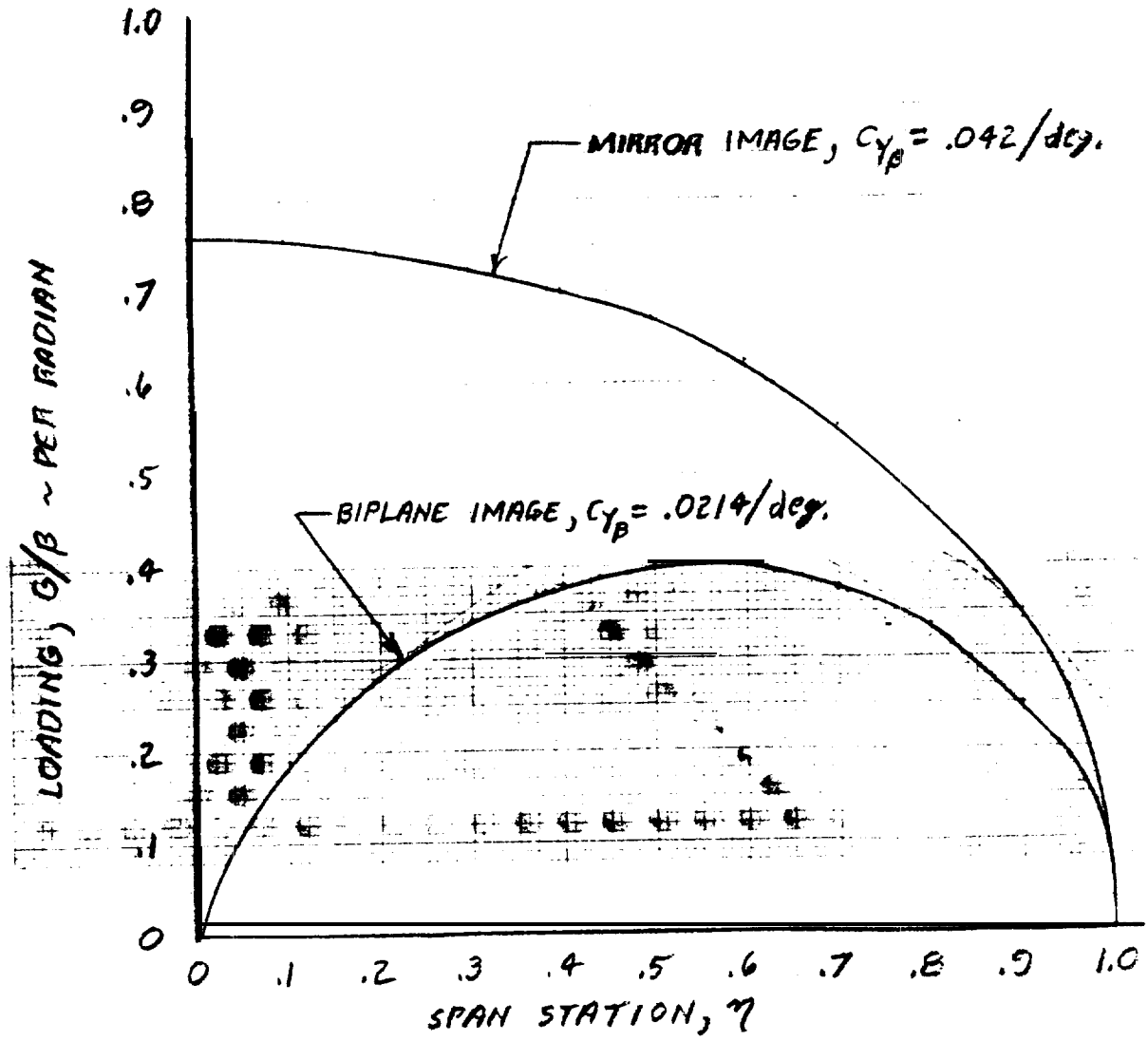

HRW 11/22/83 (G-20)

FIG. 3.4.4-2

STRUT SIDE FORCE SLOPE

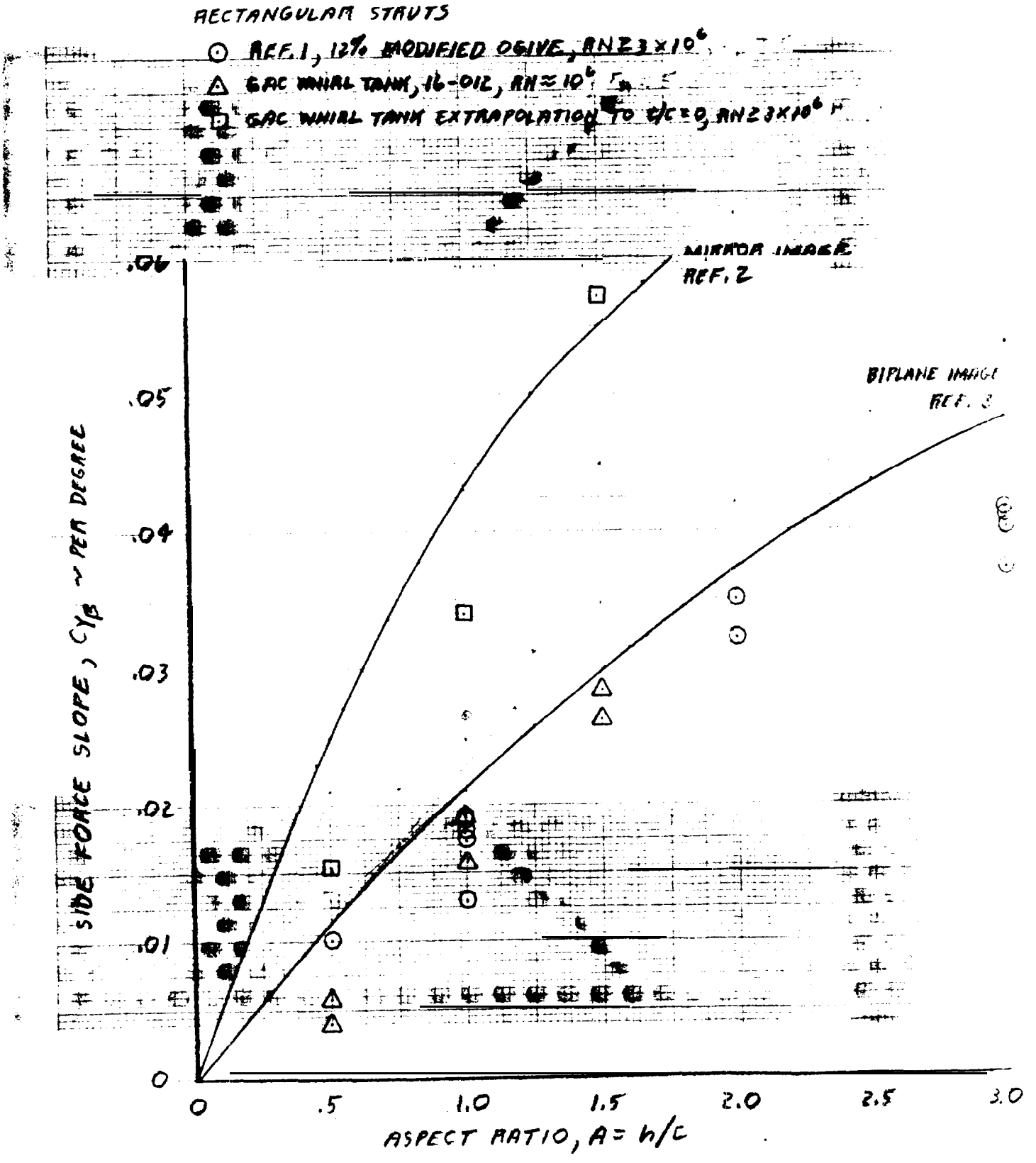

HAW 11/23/83

FIG. 3.4.4-3

STRUT SIDE FORCE SLOPE vs. THICKNESS RATIO

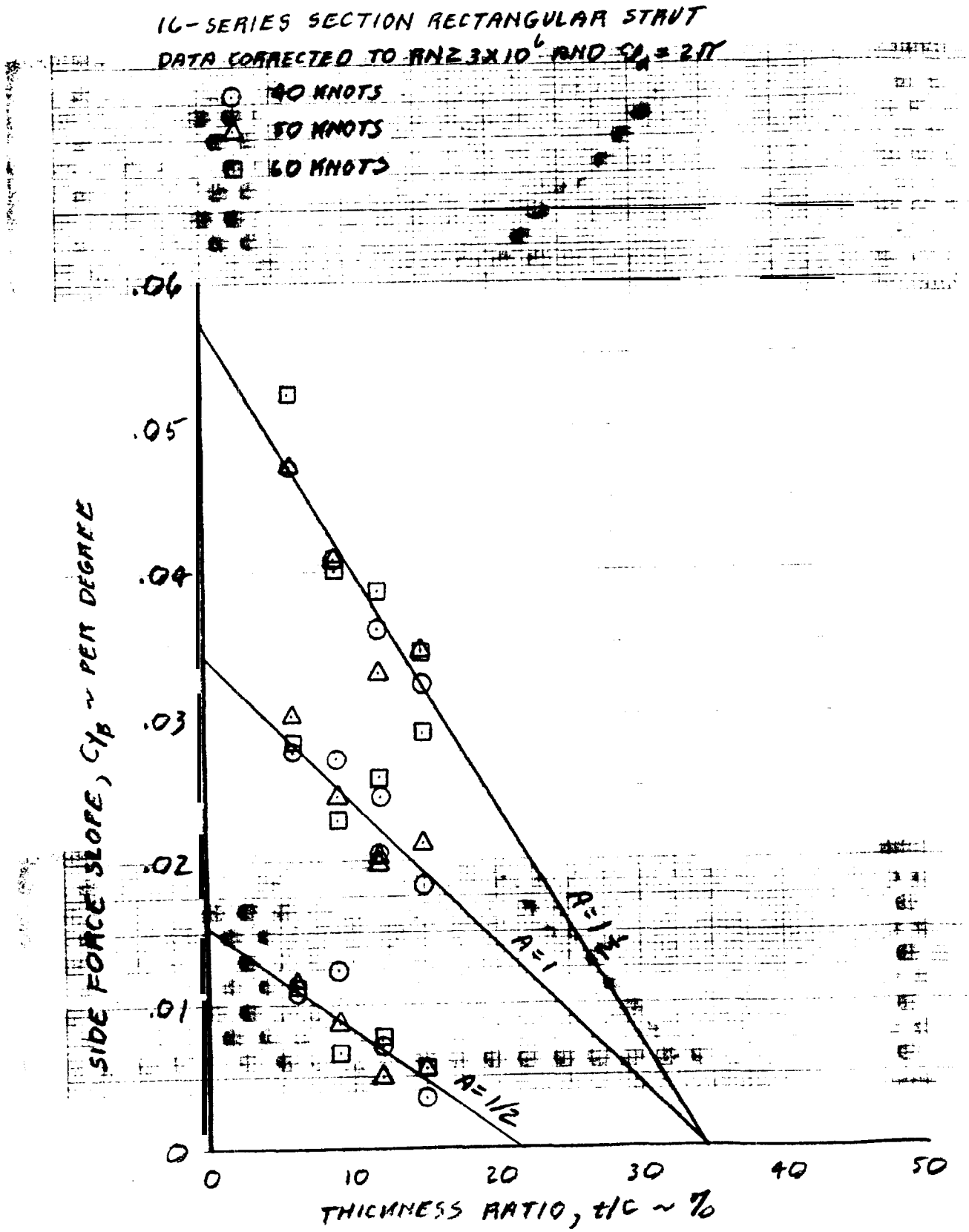

HAW 11/23/83

3.5 Foilborne Lift

3.5.1 Pitch Lift Curve Slope

Slender theory provides an adequate approximation for the pod lift increment:

$$\Delta C_{L_{\alpha_{pod}}} = 2 S_{o_{pod}} / S \qquad 3.5.1\text{-}1$$

where: $S_{o_{pod}}$ = pod frontal area

The center of pressure for the pod lift is approximately 1/3 of the forebody length aft of the pod nose:

$$a.c._{pod} = -\left(x_N - \frac{1}{3} \ell_{forebody}\right) / C_r \qquad 3.5.1\text{-}2$$

where: C_r = foil chord at foil plane of symmetry

X_N = longitudinal distance between pod nose and C_r leading edge

$\ell_{forebody}$ = pod forebody length, nose to maximum cross-section area

The foil pitch lift curve slope is then given by:

$$C_{L_\alpha} = C_{L_{\alpha_{foil}}} + \Delta C_{L_{\alpha_{pod}}} \qquad 3.5.1\text{-}3$$

where: $C_{L_{\alpha_{foil}}}$ is the foil-only pitch lift curve slope of Equation 3.4.1.1-2

$\Delta C_{L_{\alpha_{pod}}}$ is the lift curve slope increment of Equation 3.5.1-1

3.5.2 Incidence Lift Curve Slope

The incidence lift curve slope is the slope of Equation 3.4.1.1-2 for the incidence lift circulation distribution:

$$C_{L_i} = 2A \int_0^1 \frac{G}{i} d\eta \qquad 3.5.2\text{-}1$$

3.5.3 Flap Lift Curve Slope

The flap lift curve slope is given by:

$$C_{L_\delta} = \frac{d\alpha}{d\delta} C'_{L_\delta} \pm 10\% \qquad 3.5.3\text{-}1$$

where: $da/d\delta$ is the flap effectiveness of Table 3.3.1.5-I

c_{l_δ}' is the full chord flap lift curve slope of Equation 3.4.1.1-2

The nominal accuracy is that for the flap effectiveness

3.5.4 Foil Residual Lift

The foil residual lift is given by:

$$c_{L_0} \equiv c_L \text{ for } \alpha = i' = \delta = 0$$

$$= -c_{l_i'} a_{0_f} \pm c_{l_i}^{\circ}/3 \qquad \text{3.5.4-1}$$

where: $c_{l_i'}$ is the incidence lift curve slope of Equation 3.5.2-l

a_{0_f} is the section zero lift angle of Equation 3.3.1.3-2

3.5.5 Aerodynamic Foil Lift Equation

The potential value of the foil lift coefficient is:

$$c_L = c_{L_0} + (c_L)_\alpha + (c_L)_{i'} + (c_L)_\delta \qquad \text{3.5.5-1}$$

$$= c_{L_0} + c_{L_\alpha}\alpha + c_{l_i'} i' + c_{L_\delta}\delta$$

$$= c_{L_0} + c_{L_\alpha}\left(\alpha + \frac{c_{l_i'}}{c_{l_\alpha}} i' + \frac{c_{L_\delta}'}{c_{L_\alpha}} \frac{d\alpha}{d\delta}\delta\right)$$

$$= c_{L_{ref}} + (c_L)_\alpha + (c_L)_\delta \qquad \text{for rigid foil/pod intersection}$$

where c_{L_α} is the pitch lift curve slope of Equation 3.5.1-3

$c_{l_i'}$ is the incidence lift curve slope of Equation 3.5.2-l

c_{L_δ} is the flap lift curve slope of Equation 3.5.3-1

c_{L_0} is the residual lift coefficient of Equation 3.5.4-l

$c_{L_{ref}}$ is the residual lift coefficient for the case of the rigid foil/pod intersection

$$= c_{L_0} + (c_L)_{i'}$$

nominal accuracy = $\pm .05\,(c_L)_\alpha$

$\pm .1\,(c_L)_{i'}$

$\pm\, c_{l_i}^{\circ}/3$

The lift coefficient of Equation 3.5.5-l is for the inviscid, flat plate, aerodynamic (infinite depth) lift curve slope of 2π per radian. The various forms given for the equation are suited to various applications.

It must be noted that the hydrofoil circulation distribution is required for the lift coefficient distribution and cavitation characteristics. With the circulation distribution on hand it is only logical to integrate that distribution for the lift curve slope rather than resorting to one of the classic equations for slope which are emperical approximations for that integral. However, a brief review of the relationship between the pitch lift circulation integral and the classic lift curve slope equations provides a foundation for the consideration of more complex hydrofoil characteristics.

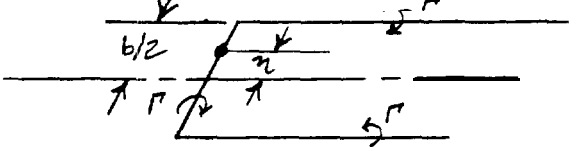

The uniformly loaded lift line is frequently employed for illustration in the hydrofoil literature because it presents the most elementary possible view of the foil. In this view the lift coefficient is given by:

$$C_L = \frac{2\Gamma}{V C_{avg}} \int_0^1 d\eta = \frac{2\Gamma}{V C_{avg}} \qquad 3.5.5\text{-}2$$

$$\Gamma = \frac{1}{2} C_L V C_{avg}$$

Then the downwash at station η is:

$$w_\eta = \frac{\Gamma}{4\pi \frac{b}{2}(1-\eta)} + \frac{\Gamma}{4\pi \frac{b}{2}(1+\eta)}$$

$$= \frac{\Gamma}{\pi b} \frac{1}{1-\eta^2} \qquad 3.5.5\text{-}3$$

and the induced angle is:

$$\alpha_{i_\eta} = \frac{w_\eta}{V} = \frac{\Gamma}{\pi b V} \frac{1}{1-\eta^2} = \frac{C_L C_{avg}}{2\pi b} \frac{1}{1-\eta^2}$$

$$= \frac{C_L}{2\pi A} \frac{1}{1-\eta^2} \qquad 3.5.5\text{-}4$$

The averaged induced angle of Equation 3.5.5-4 is not defined because of the singularity at the foil tip but averaged over 96% of the span, which is about the point at which the free vortex becomes rotational, the induced angle becomes $C_L / \pi A$.

The uniform circulation distribution is an abstraction; circulation distributions tend to be elliptical and particularly so for hydrofoils, The derivation for the downwash produced by an elliptically loaded lift line is tedious but classic; a detailed derivation is given in Reference 1. The result gives a constant downwash on the span having the value:

$$w = \frac{\Gamma_0}{2b} \qquad 3.5.5\text{-}5$$

and from Eauation 3.4.1-/and 3.4.1.1-1:

$$w = \frac{2 C_L b V}{2b \pi A} = \frac{C_L V}{\pi A}$$

$$\alpha_i' = \frac{w}{V} = \frac{C_L}{\pi A} \qquad 3.5.5\text{-}6$$

The literature offers many demonstrations that this is the minimum induced angle possible. For this induced angle the foil lift curve slope becomes:

$$\alpha = \alpha_0 + \alpha_i'$$

$$= \frac{C_L}{C_{l_\alpha}} + \frac{C_L}{\pi A}$$

$$\alpha_{C_L} \equiv \frac{d\alpha}{dC_L} = \frac{1}{2\pi} + \frac{1}{\pi A} = \frac{A+2}{2\pi A}$$

$$C_{L_\alpha} = dC_L/d\alpha = \frac{2\pi A}{A+2} \qquad 3.5.5\text{-}7$$

which is the familiar elliptically loaded lift line result.

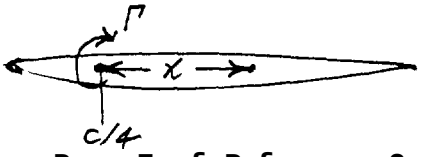

As presented on Page 7 of Reference 2, the downwash distribution on the section is given by:

$$w_x = \frac{\Gamma}{2\pi x} \qquad 3.5.5\text{-}8$$

where the circulation is related to the section lift coefficient by:

$$L = \rho \Gamma V b = c_l \frac{\rho}{2} V^2 c b$$

$$\Gamma = \frac{c_l c V}{2} \qquad \text{3.5.5-9}$$

From Equations 3.5.5-B and -9:

$$c_{l_\alpha} = 2\pi K = \frac{c_l}{w/V}$$

$$= \frac{2\Gamma}{cV} \Big/ \frac{\Gamma}{2\pi x V}$$

$$= 4\pi \frac{x}{c}$$

$$\frac{x}{c} = \frac{1}{2} K \qquad \text{3.5.5-10}$$

That is, for a section lift curve slope of 2π (K=1) the downwash must be measured ½ chord behind the quarter-chord point to properly relate the circulation to the section angle of attack. this refinement increases the induced angle obtained from lift line calculations such as those of Equations 3.5.5-4 and -7.

DeYoung's procedure, which makes the flow tangent to the surface at the three-quarter-chord line at seven points on the span is about the limit for a desk calculation and provides all the precision available to the state of the art.

In lifting surface theory, then, the average induced angle becomes some constant, say $c_1/2$, times the elliptically loaded lift line value of Equation 3.5.5-6:

$$\alpha_i = \frac{c_1/2}{\pi A} C_L \qquad \text{3.5.5-11}$$

and the lift curve slope of Equation 3.5.5-7 becomes:

$$a = \frac{c_l}{2\pi} + \frac{c_1/2}{\pi A} C_L \qquad \text{3.5.5-12}$$

$$\alpha_{C_L} = \frac{A + c_1}{2\pi A}$$

$$C_{L_\alpha} = \frac{2\pi A}{A + c_1}$$

For comparison with the slopes derived from lifting surface theory Equation 3.5.5-12 may be written:

$$\frac{2\pi A}{C_{L\alpha}} = A + C_i \qquad 3.5.5\text{-}13$$

Figure 3.5.5-l is adapted to the form of Equation 3.5.5-13 from Figures 4, 10, and 11 of Reference 2. The figure shows that the lift curve slope for elliptically loaded foils of aspect ratio greater than about 3 is approximately given by:

$$C_{L\alpha} = \frac{2\pi A}{A + 2.75} \qquad 3.3.5\text{-}14$$

Pope notes on Pg. 207 that velues of 2.5 to 3.0 are employed for the constant.

Pope employed a .4 taper ratio on an unswept foil to approximate the elliptical loading and this planform should be compared with Figure 3.4.2.1-2. Inverted "T" hydrofoils employ the lowest taper ratio that will not unduly increase the C_{ℓ}/C_L ratio for structural reasons with some sweep to clear the leading edge of debris. The .25 taper ratio and 15° sweep of Figure 3.5.5-l is typical of such foils and Equation 3.5.5-14 would therefore be typical for the inverted "T" configuration.

For the general, non-elliptic loading, case the foil lift curve is a very complex function of the planform. The DATCOM and ESDU equations for this relationship are very different in form but produce practically identical results when evaluated for the .25 taper ratio, 15° sweep case of Figure 3.5.5-l as shown on Figure 3.5.5-2.

Pope introduces the Jones edge correction Factor, E, on Pg. 207 and incorporates it into Equation 3.5.5-7 to obtain his Equation (10.36) for an elliptic wing (elliptic loading):

$$C_{L_\alpha} = \frac{2\pi A}{AE + 2} \qquad 3.5.5\text{-}15$$

where E = semi-perimeter/span

$$= \frac{\pi A + 4}{16A} \quad \frac{4 - 3\varepsilon^2}{1 - \varepsilon} \qquad \text{for ellipse}$$

where $\varepsilon = \frac{1}{4}\left(\frac{\pi A - 4}{\pi A + 4}\right)^2$

Equation 3.5.5-15 is shown on Figure 3.5.5-1. Pope's discussion of E is intuitive and the discussion of Reference 7 only points out that there are several definitions for the factor. It is quite likely that Equation 3.5.5-15 is, like Equation 3.5.5-14, a simple curve fit to results obtained by better founded and much more complex theory.

Pope goes on to introduce the classic lift slope τ factor in his Section 10.10. The Gibbs and Cox Equation (2.34) is identical with Pope's Equation (10.44) except for the incorporation of sweep into the Gibbs and Cox equation:

$$C_{L_\alpha} = \frac{2\pi A \cos\Lambda}{AE + 2(1+\tau)\cos\Lambda} \qquad 3.5.5\text{-}16$$

This equation is also shown on Figure 3.5.5-2. The τ factor is well founded but does not produce the lifting surface result for elliptic loading without the E factor. Thus equation 3.5.5-16 is another curve fit.

If the section lift curve slope is less thant 2π, as is usally the case, the control point of Equation 3.5.5-10 should move forward of the three-quarter chord point. DeYoung's procedure makes this adjustment and the $C_{L_{S_I}}$ of Equation 3.4.1.1-2 are actually $\frac{C_{L_{S_I}}}{K}$.

The K factor appears in the theoretical lift curve slopes of DATCOM, ESDU, and References I and 7 in particular and in Equation 3.5.5-12 as:

$$\alpha = \frac{C_L}{2\pi K} + \frac{C_i/2}{\pi A} C_L \qquad 3.5.5-16A$$

$$\alpha_{C_L} = \frac{A + K C_i'}{2\pi A K}$$

$$C_{L_\alpha} = \frac{2\pi A K}{A + K C_i'}$$

$$\text{or} \quad \frac{2\pi A K}{AE + 2K(1+T)}$$

Many forms of Equation 3.5.5-16 incorporating various definitions for E and κ appear in the literature and that flexibility has been employed to correlate experimental data. In fact, lifting surface theory cannot be summarized in such a simple equation and such correlations must be regarded as curve fits rather than as confirmations of theory.

The HANDE aerodynamic lift curve slope is given in Section 8.2.2.3 of Reference 8. For a section lift curve slope of $2\pi\kappa$ that equation can be written:

$$C_{L_{\alpha_{wb}}} = \frac{2\pi A}{\sqrt{\frac{A^2}{\kappa^2 \cos^2 \Lambda} + 4} + 2} \qquad 3.5.5\text{-}17$$

which provides the potential value for the foil lift curve slope for κ=1.0. Equation 3.5.5-17 is presented graphically on Figure 3.5.5-3.

No statistically significant measure of the accuracy for DeYoung's procedure can be offered and the nominal accuracies of Equation 3.5.5-l are those for the section from Section 3.3.1. Figure 12 of Reference 2 is generally consistent with the ±5% nominal accuracy for slope but includes two cases for which the predicted slope was 20% low. More than lift surface theory is involved anyway; the lift curve prediction includes accountability for pod lift, section thickness and thickness distribution, and Reynolds Number. The Reynolds Number presents a particular problem in establishing the accuracy for a lift curve prediction because most of the data is model data and the lift, drag, and moment data must be examined to determine the extent of the laminar flow.

In summary, Equation 3.5.5-l will serve as an estimate for the foil lift curve and Equation 3.5.5-14 can be employed as a check on the pitch lift circulation distribution for planforms offering near-elliptic distributions. Model measurements falling outside the accuracy range of Equation 3.5.5-l should be examined for evidence of an abnormal transition point.

REFERENCES

1. Pope, Alan, "Basic Wing and Airfoil Theory," McGraw-Hill, 1951.
2. DeYoung, J. and C.W. Harper, "Theoretical Symmetric Span Loading at Subsonic Speeds for Wings Having Arbitrary Plan Form," NACA Report 921, 1948.
3. Krienes, K., "The Elliptic Wing Based on The Potential Theory," NACA TM 971, 1941.
4. Swanson, R.S. and E.L. Priddy, "Lifting-Surface-Theory Values of the Damping in Roll and of the Parameter Used in Estimating Aileron Stick Forces," NACA ARR L5F23, 1945.
5. Zimmerman, C.H., "Characteristics of Clark Y Airfoils of Small Aspect Ratios," NACA Report 431, 1932.
6. Lange and Wacke, "Test Report on Three and Six-Component Measurements on a Series of Tapered Wings of Small Aspect Ratio (Partial Report: Triangular Wing)," NACA TM 1176, 1948.
7. Michel, W.H., S.F. Hoemer, L.W. Ward, and T.M. Buermann, "Hydrofoil Handbook Vol. II, Hydrodynamic Characteristics of Components," Bath Iron Works Corp. by Gibbs and Cox, Inc., 1954.

a. HANDE Staff, "Hydrofoil Analysis and Design Program (HANDE) Theory Manual," Vol II, Boeing Company Document No. D321-51312-2, 2 July 1976.

FIG. 3.5.5-1

PARAMETRIC LIFT CURVE SLOPE

- ○ MAXIMUM SLOPE OF KRIENES AND SWANSON, PRIDDY FOR ELLIPTIC DISTRIBUTION, REFS. 3 & 4
- ◇ $\lambda = .4, \Lambda = 0$
- □ RECTANGULAR WINGS } DeYOUNG
- △ TRIANGULAR WINGS }
- ■ ZIMMERMAN, RECTANGULAR WING MEASUREMENTS, REF. 5
- ▲ LANGE & WACKE, TRIANGULAR WING MEASUREMENTS, REF. 6
- × DeYOUNG, $\lambda = .25, \Lambda = 15°$

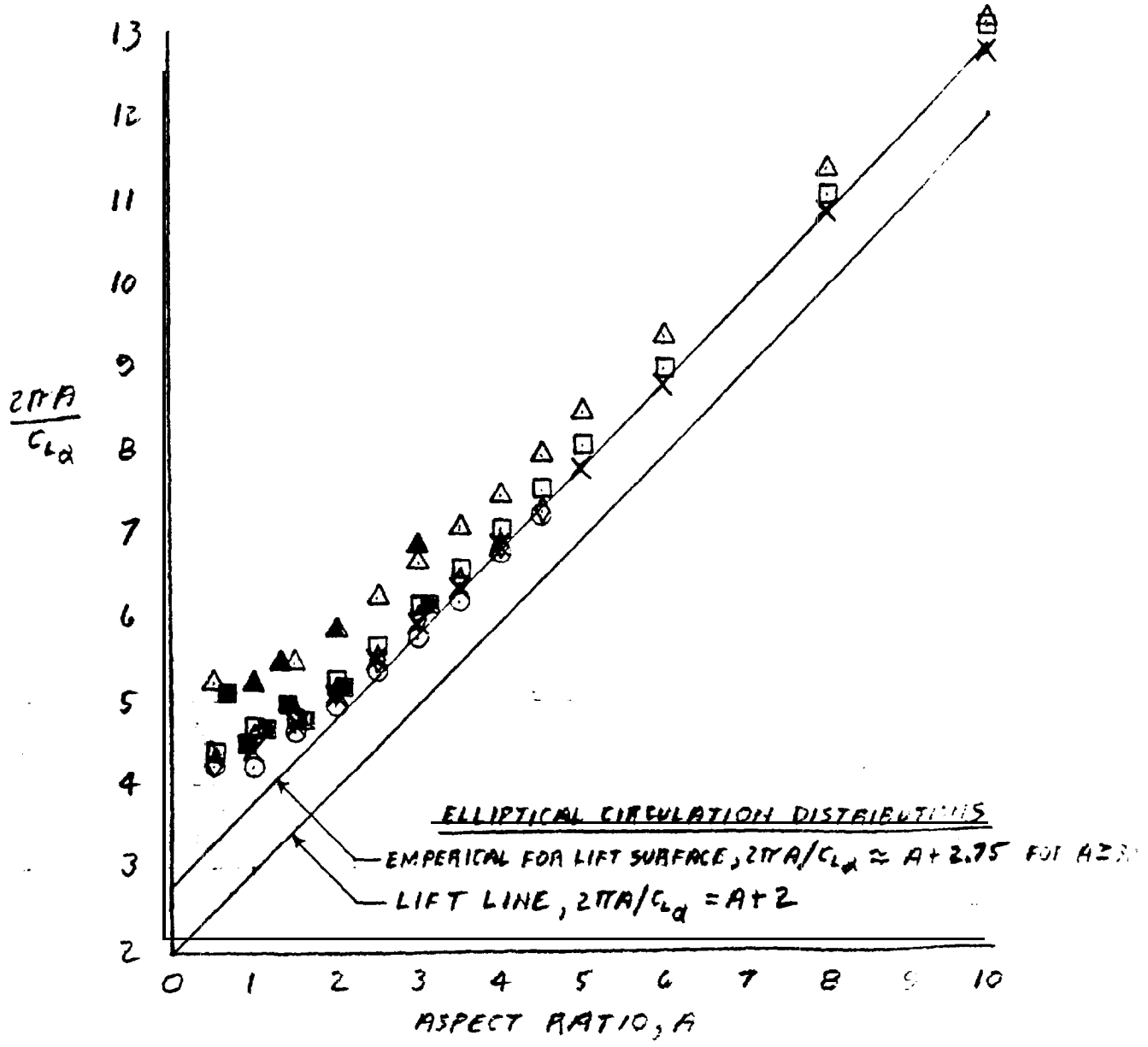

HFW 12/19/63

FIG. 3.5.5-2

LIFT CURVE SLOPE ESTIMATE

$\lambda = .25$ $\Lambda = 15°$

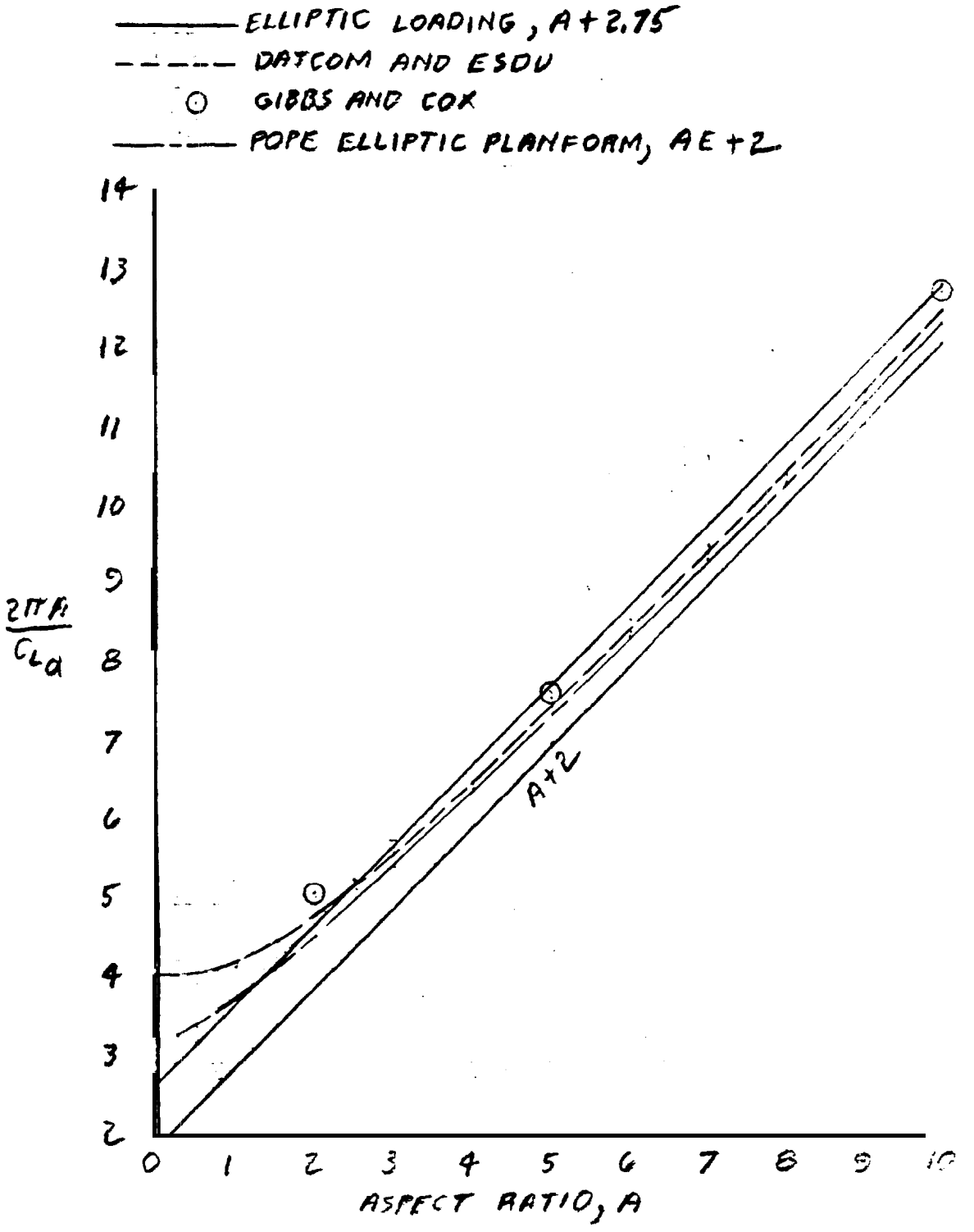

HRW 12/15/23

FIG. 3.5.5-3

HANDE AERODYNAMIC LIFT CURVE SLOPE

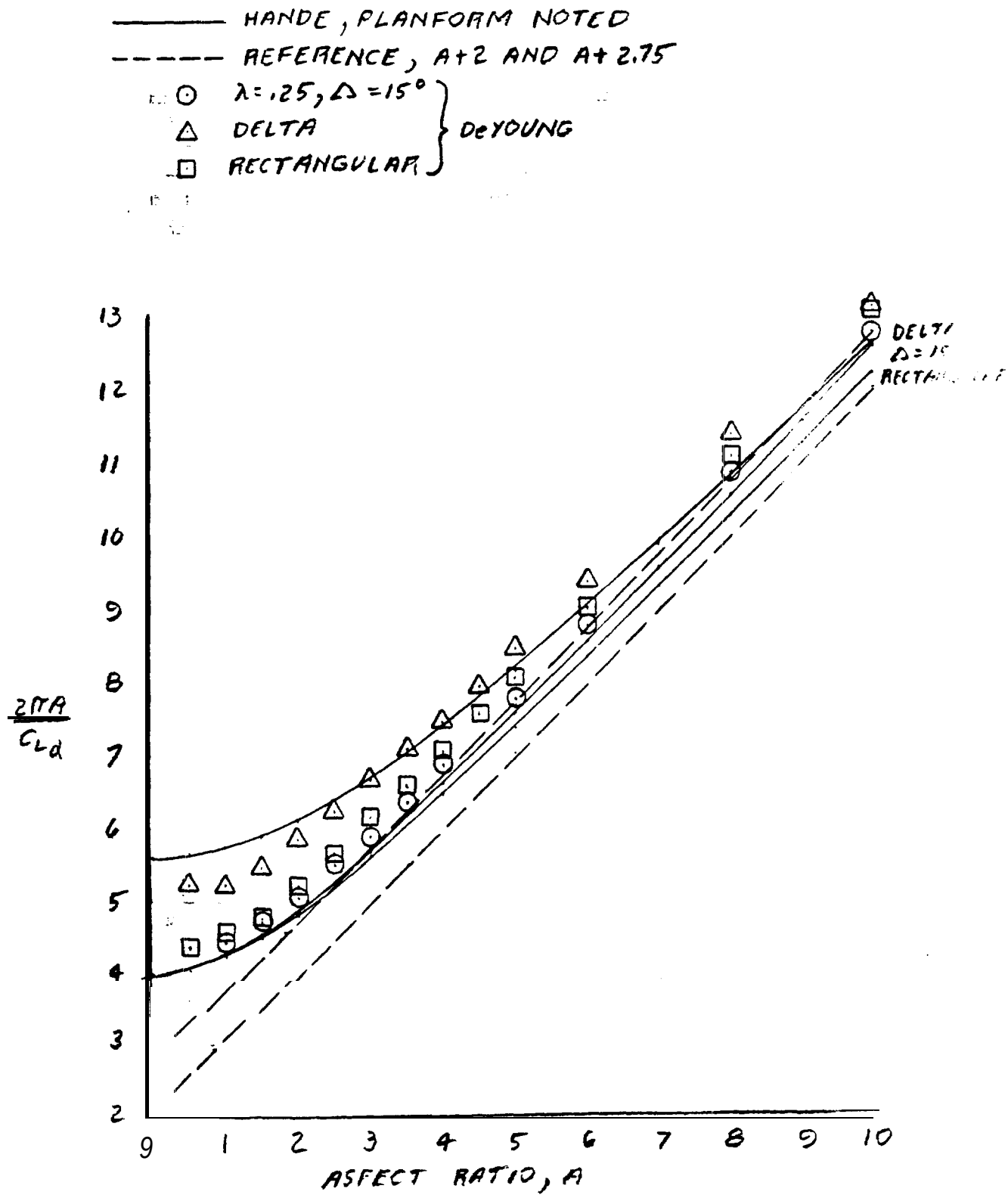

HTW 9/5/84

3.5.6 Free Surface Effect

GENERAL

Three dimensional free surface effects present forbidding academic and experimental problems. Model and prototype measurement does not yet provide evaluation of theory, much less guide development of that theory. The most intense academic studies still must resort to certain approximations and this discussion is limited to those studies which carry those approximations to a point which allows explicit expression for the results; academicians should refer to the source classics such as References l-3.

The two dimensional hydrodynamic lift curve slope is given by Equation 3.3.7. 1-19 which may be written:

$$a_{c_l} = a_{c_{l_\alpha}} + a_{c_{l_\alpha}} \frac{\pi}{(4\frac{h}{c})^2 + 1} + a_{c_{l_\alpha}} \times 2\pi \frac{f(F_n)}{h/c}$$

$$= \frac{1}{2\pi K} + \frac{\pi}{K} a_{c_{l_{A=\infty}}} + \frac{1}{K} a_{c_{l_{WA=\infty}}} \qquad \text{3.5.6-l}$$

The first term of Equation 3.5.6-l is the inverse aerodynamic lift curve slope of Equation 3.3.7.1-19 and establishes a logical section chord station for the measurement of downwash and induced angle effects as noted in Equation 3.5.5-10. In fact that reference chord station is generally assumed to be the 3/4 chord station, K=1, as in the second term of Equation 3.5.6-l which measures the downwash at the section 3/4 chord station due to the lift line free surface image. Lift line theory identifies the angular reference station with the lift line itself at the quarter-chord station.

The third term of Equation 3.5.6-l is not a downwash evaluation at all but an inference which expresses the Kochin lift line wave drag in the form of an induced angle. For the derivation of the induced angle terms of Equation 3.5.6.1-1 the K factor has a doubtful quantitative significance in those terms but it is required for consistency with Equation 3.3.7.1-19.

The three dimensional foil requires accountability for the finite extent of the image bound vortex, for the addition of the free vortex system and its image, and for the effect upon the wave induced angle of the finite extent of the lift line and of the addition of the free vortices. The effect of the horseshoe vortex system consisting of the finite bound vortex and the added free vortices is already available in Equation 3.5.5-12 and the first term of Equation 3.5.6.1-1 can be replaced by:

$$\alpha_{C_{L_0}} = \frac{A + C_i'}{2\pi K A} = \frac{1}{2\pi K} + \frac{C_i'}{2\pi K A} \qquad 3.5.6\text{-}2$$

where accountability for section geometry and viscous effect has been supplied in equation 3.5.5-12.

IMAGE BOUND VORTEX

For a uniform circulation distribution on a rectangular foil the distribution of the downwash on the 3/4 chord line due to the finite image bound vortex is given by:

$$\frac{\alpha_B}{C_L} = \frac{w_B}{V C_L} = \frac{A}{4\pi\left[(4\frac{h}{c})^2+1\right]}\left[\frac{1-\eta}{\sqrt{(4\frac{h}{c})^2+1+A^2(1-\eta)^2}} + \frac{1+\eta}{\sqrt{(4\frac{h}{c})^2+1+A^2(1+\eta)^2}}\right] \qquad 3.5.6\text{-}3$$

which is illustrated on Figure 3.5.6-l. The value of this distribution at mid-span is Wadlin's W_2 which is referenced to the mid-span value of the aeordynamic downwash in Reference 4 to obtain the free surface effect as a

proportionality, Gibbs and Cox employs the **more** generally **appropriate averaged value of this distribution in Reference 5:**

$$\alpha_{C_{L_C}} = \left[\sqrt{\left(4\frac{h}{c}\right)^2+1+4A^2} - \sqrt{\left(4\frac{h}{c}\right)^2+1}\right] \Big/ 4\pi A\left[\left(4\frac{h}{c}\right)^2+1\right] \qquad \text{3.5.6-4}$$

which reduces to the $\alpha_{C_{L_C}}$ **of Equation 3.5.6-l for the infinite aspect ratio case.**

Evaluated at the lift line, as in References 1 and 6, the image bound vortex produces a speed reduction and lift curve non-linearity of little **practical significance as noted under Equation 3.3.7.1-12.**

Equation 3.5.6-4 is the only authoritative measure of the image bound vortex effect which can be offered here but it should be noted that this equation is for the particular case of the uniform circulation distribution, which is an abstraction, and the rectangular planform.

IMAGE **FREE VORTEX SYSTEM**

For the foil free vortices, which have no 'lateral **motion,** Kochin's **equation would seem to** call **for free surface mirror images. The question has been discussed in Section 3.4.4 in connection with the strut free vortices but *in* the foil context the literature universally employs the biplane image, presumably because the free vortex mirror image would produce a discontinuous image system in violation of** Helholtz'**first law.**

For a uniform circulation distribution on a rectangular foil the distribution of the downwash **due to the biplane image free vortices may be written:**

$$\frac{\alpha_F}{C_L} = \frac{w_F}{VC_L} = \left\{\frac{1-\eta}{4\pi A\left[\left(4\frac{h}{b}\right)^2+(1-\eta)^2\right]} + \frac{1+\eta}{4\pi A\left[\left(4\frac{h}{b}\right)^2+(1+\eta)^2\right]}\right\} \qquad \text{3.5.6-5}$$

$$+\left\{\frac{1-\eta}{4\pi A\left[\left(4\frac{h}{b}\right)^2+(1-\eta)^2\sqrt{\left(4\frac{h}{c}\right)^2+1+A^2(1-\eta)^2}\right.}\right.$$

$$\left.\left. + \frac{1+\eta}{4\pi A\left[\left(4\frac{h}{b}\right)^2+(1+\eta)^2\right]\sqrt{\left(4\frac{h}{c}\right)^2+1+A^2(1+\eta)^2}}\right\}\right.$$

$$= \left(\frac{\alpha_F}{C_L}\right)_{C/4} + \Delta\left(\frac{\alpha_F}{C_L}\right) \qquad \text{3.5-16}$$

Equation 3.5.6-5 is illustrated on Figure 3.5.6-2. The form of the equation distinguishes the downwash angles as evaluated on the quarter-chord line, the lift line, and on the 3/4 chord line. Wadlin employs the mid-span value for this distribution relative to the mid-span value of the aerodynamic downwash though the average value carries more absolute significance.

The average value for this distribution as evaluated at the quarter-chord line is given by:

$$\frac{\alpha_F}{C_L} = \ln \sqrt{\frac{1}{4\left(\frac{h}{b}\right)^2} + 1} \Big/ 4\pi A \qquad 3.5.6\text{-}6$$

No explicit expression can be offered here for the average value for this downwash as evaluated at the 3/4 chord line. The distributions were integrated numerically here. These averages are illustrated on Figure 3.5.6-3 in the parametric form $\pi A \alpha_F / C_L$. It will be noted that in this form the average values evaluated at the quarter-chord line, Equation 3.5.6-6, are independent of aspect ratio.

The uniform circulation distribution is an abstraction but analysis of free vortex image induced angle for a non-uniform circulation distribution presents severe mathematical problems. Prandtl derived the average induced angle evaluated at the lift line for an elliptic circulation distribution and expressed the result as a fraction of the aerodynamic induced angle, i.e., Prandtl's biplane factor is:

$$\sigma_i' = \frac{\alpha_F}{C_L} \Big/ \frac{\alpha_i'}{C_L} = \frac{\alpha_F}{C_L} \Big/ \frac{C_i'}{2\pi A} \qquad 3.5.6\text{-}7$$

$$= \pi A \alpha_F / C_L$$

for theoretical aerodynamic induced angle for elliptic lift distribution

The biplane factor is designated K_b-1 in the Gibbs and Cox handbook where K_b is presented grapahical Jy. There is *a* rather awkward parametric formulation for the factor given with its derivation in Reference 7. Wilson presents a more compact formula due to Wu and a table of values for the factor which is included here 'in Table 3.5.6-I. Wilson also suggests a polynomial approximation which is convenient for pocket computers and which represents Wu's equation within .05% to a depth of .8 spans and within .2% to a depth of one span:

$$\alpha_i = 1 - \frac{8}{\pi}\frac{h}{b}\sqrt{1+4\left(\frac{h}{b}\right)^2}\left[.38629 - .35104 m_1 - .035251 m_1^2 + (.5 - .12392 m_1 - .012377 m_1^2)\ln\frac{1}{m_1}\right] \qquad 3.5.6\text{-}8$$

where: $m_1 = \dfrac{1}{1+\sqrt{1+4(h/b)^2}}$

The biplane factor is compared with the induced angles of Figure 3.5.6-3 on Figure 3.5.6-4.

No confidence level has been established for the biplane factor. The elliptic circulation distribution is certainly more representative of the hydrofoil than is the uniform circulation distribution but evaluation at the lift line does not present the full effect of the image free vortices. Figure 3.5.6-3 indicates that, for the uniform circulation distribution, evaluation at the 3/4 chord line increases the induced angle about 15%. Taper and sweep introduce further uncertainties but the application of the biplane factor introduces the greatest uncertainty. The biplane factor presents the image induced angle as a fraction of the theoretical aerodynamic induced angle, $1/\pi A$. Figure 3.5.5-l indicates that applying that factor to the practical aerodynamic induced angle will increase the induced angle 35%-50% and that $\sigma_i/\pi A$ would provide a better estimate for this angle.

WAVE INDUCED ANGLE

Wilson presents the total free surface drag coefficient as the sum of a depth dependent and Froude number dependent term:

$$C_{D\,free\ surface} = C_{D\,surf} + C_{D\,wave} = C_{D\,Si} + C_W$$
$$= -\frac{\sigma_i'}{\pi A} C_L^2 + C_W \qquad 3.5.6\text{-}9$$

It is interesting to note that the depth term, $C_{D\,Si}$, presents a mirror image for the free surface. At zero Froude number the C_W term vanishes leaving the mirror image induced angle as the total free surface effect, which is wholly consistent with the intuitive interpretation of Kochin's result as applied to the free vortices. At infinite Froude number the C_W coefficient has the value $2\sigma_i' C_L^2/\pi A$, producing the biplane image induced angle as the total free surface effect.

The C_W term is very idfficult to evaluate; Wilson presents a computer program for this evaluation which is quite sophisticated even for the idealized case considered. In pursuit of a convenient explicit expression for the free surface drag the Gibbs & Cox handbook presented that drag as the sum of the biplane image drag and a drag proportional to the two dimensional wave drag. From evaluation of the theoretical free surface drag for an aspect ratio 10 foil at a depth of .84 chords, one of the cases of Reference 4, the biplane factor, σ_i', was tentatively selected for the constant of proportionality, i.e.:

$$\frac{C_{D_{FS}}}{C_L^2} = \frac{C_{D\,surf}}{C_L^2} + \sigma_i' \frac{f(F_h)}{h/c}$$
$$= \frac{\sigma_i'}{\pi A} + \sigma_i' \frac{f(F_h)}{h/c} = \frac{C_W}{C_L^2} - \frac{\sigma_i'}{\pi A} \qquad 3.5.6\text{-}N$$

Figures 3.5.6 -5 and -6 indicate that σ_i' serves equally well for the aspect ratio 6 foil at practical depths and Froude numbers but Figure 3.5.6-6 should

be prepared for all of the evaluations offered by Wilson to establish the limitations on this approximation.

Identifying the wave induced drag coefficient with the induced angle in the manner of Reference 5, the wave induced angle becomes:

$$\frac{\alpha_{wave}}{C_L} = \frac{C_{Dwave}}{C_L^2} = \sigma_1 \frac{f(F_h)}{h/C} \qquad 3.5.6\text{-}11$$

It must be noted that the disassociation of the free surface effect into biplane image and wave components is a convenience, having only intuitive significance.

REFERENCES

1. Wu, Y.T., "A Theory for Hydrofoils of Finite Span," California Institute of Technology Hydrodynamics Laboratory Report No. 26-8, May 1953.
2. Breslin, J.P., "A Linearized Theory for the Hydrofoil of Finite Span in a Fluid of Infinite Depth," Bath. Iron Works Corp. by Gibbs & Cox, Inc. Technical Report No. 16, Jan. 1954.
3. Breslin, J.P., "Applications of Ship-Wave Theory to the Hydrofoil of Finite Span," SNAME Journal of Ship Research, Vol. 1, No. 1, 1957, P. 27.
4. Wadlin, K.L., C.L. Shuford, Jr. and J.R. McGehee, "A Theoretical and Experimental Investigation of the Lift and Drag Characteristics of Hydrofoils at Subcritical and Supercritical Speeds," NACA Report 1232, 1955.
5. Michel, H.W., S.F. Hoerner, L.W. Ward, and T.M. Buermann, "Hydrofoil Handbook Vol. II, Hydrodynamic Characteristics of Components," Bath Iron Works Corp. by Gibbs & Cox, Inc., 1954.

6. Wilson, M.B., "Lifting Line Calculations for Hydrofoil Performance at Arbitrary Froude Number and Submergence; Part 1, Fixed Shape Elliptical Circulation Distribution," DTNSRDC SPD-0839-01, June 1978.

7. Durand, W.F., Editor-in-Chief, Th. von Karman, and J.M. Burgers, "Aerodynamic Theory" Vol. II, "General Aerodynamic Theory-Perfect Fluids," Chapt. IV, Section 18, Dover, 1963.

TABLE 3.5.6 – I

BIPLANE FACTOR, σ_i

From Table 4, Reference 6

h/b	σ_i
0	1
.005	.9364
.01	.8906
.015	.8513
.02	.8163
.025	.7845
.03	.7553
.04	.7027
.05	.6565
.075	.5604
.1	.4842
.125	.4221
.15	.3705
.175	.3273
.2	.2905
.225	.2592
.25	.2322
.275	.2089
.3	.1886

h/b	σ_i
.325	.17095
.35	.1555
.375	.1418
.4	.1298
.425	.1191
.45	.1096
.475	.1011
.5	.09351
.6	.06999
.7	.05406
.8	.04285
.9	.03472
1	.02865
1.25	.01889
1.5	.01334
1.75	.009904
2	.007635
2.25	.006061
2.5	.004927

FIG. 3.5.6 -1

IMAGE BOUND VORTEX

INDUCED ANGLE DISTRIBUTION

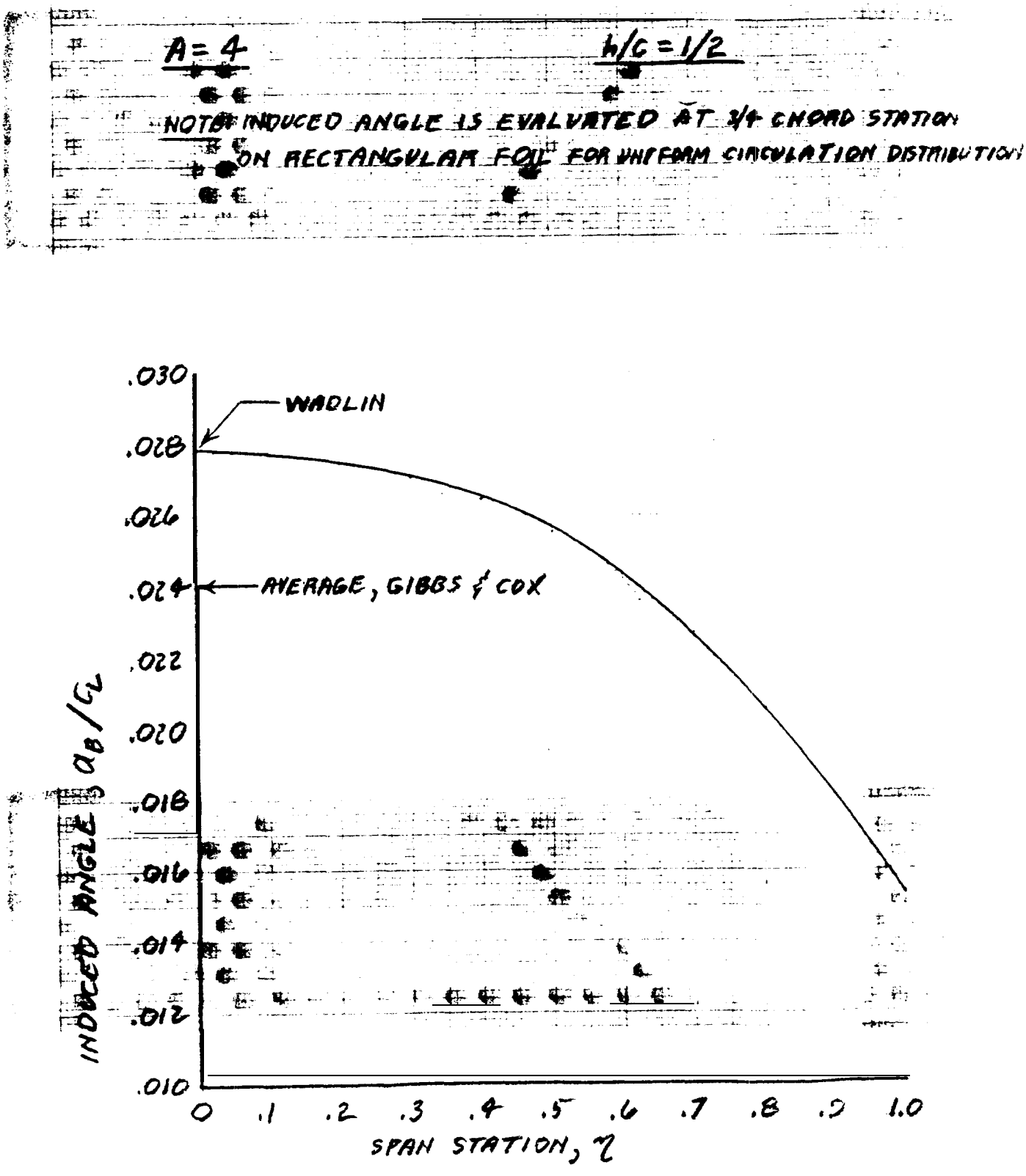

HRW 9/10/84

FIG. 3.5.6 -2

IMAGE FREE VORTEX SYSTEM

INDUCED ANGLE DISTRIBUTION

A = 4 & 10 $\quad$ h/c = 1/2

NOTE: UNIFORM CIRCULATION DISTRIBUTION ON RECTANGULAR FOIL

——— EVALUATED AT 3/4 CHORD LINE

- - - - EVALUATED AT 1/4 CHORD LINE

NOTE: WADLIN EMPLOYS MID-SPAN VALUE EVALUATED AT 3/4 CHORD LINE

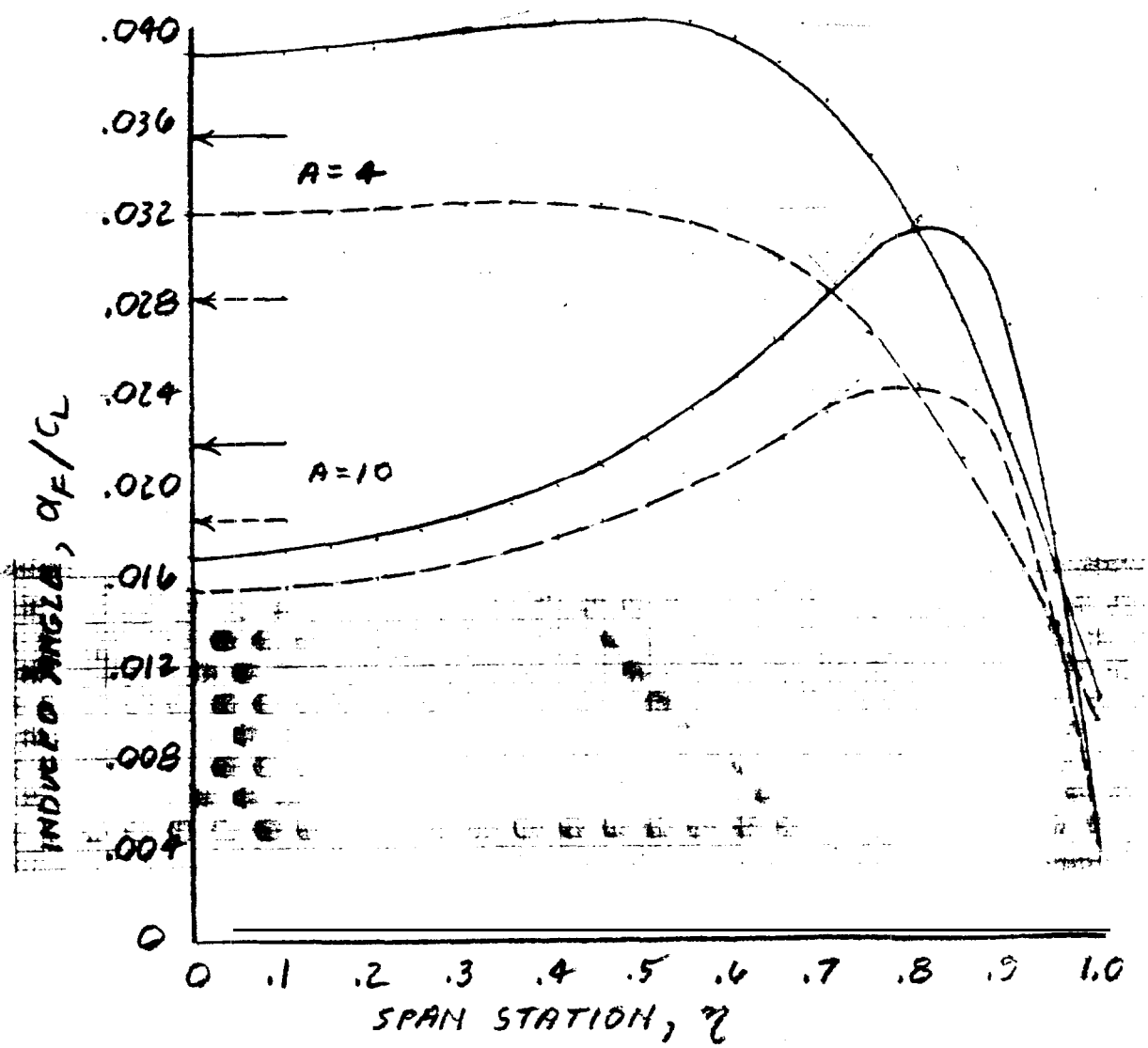

HRW 9/12/84

FIG. 3.5.6 -3

IMAGE FREE VORTEX SYSTEM

AVERAGE INDUCED ANGLE

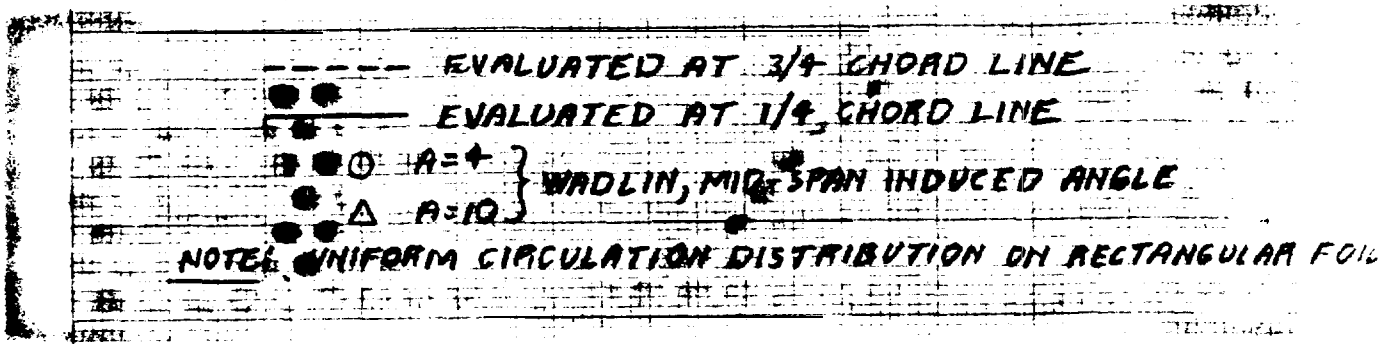

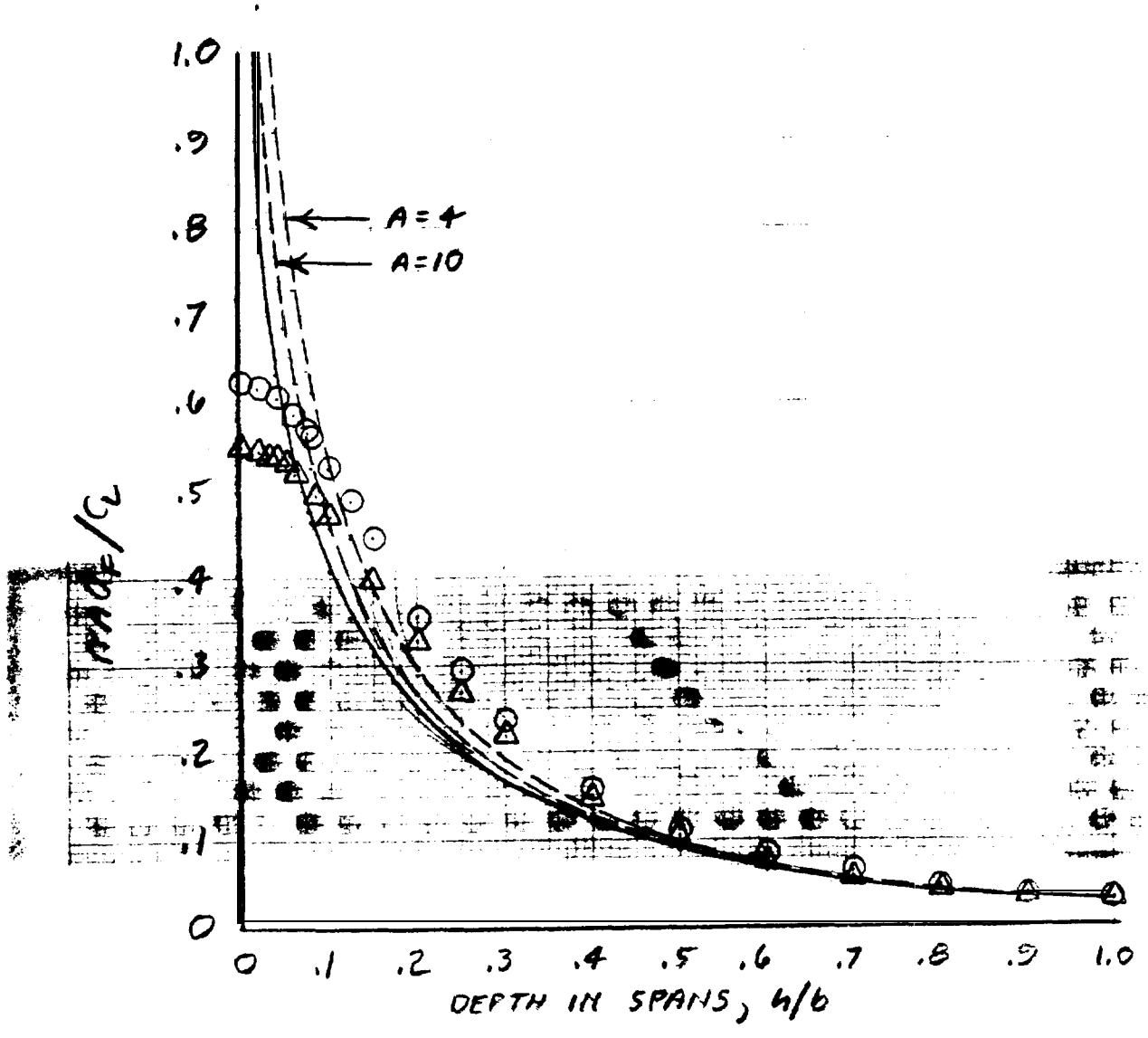

HRW 4/12/84

FIG. 3.5.6 – 4

BIPLANE FACTOR, σ_i

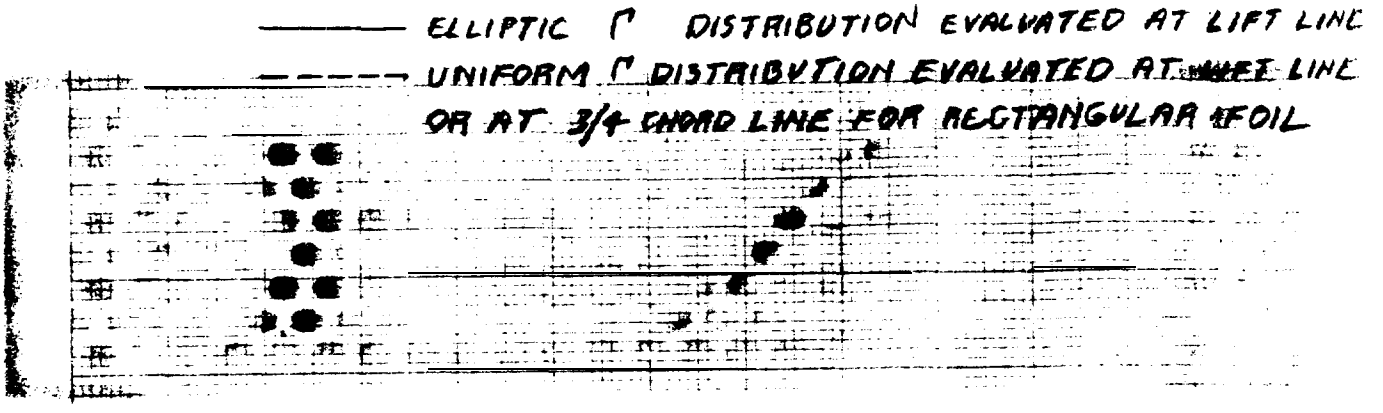

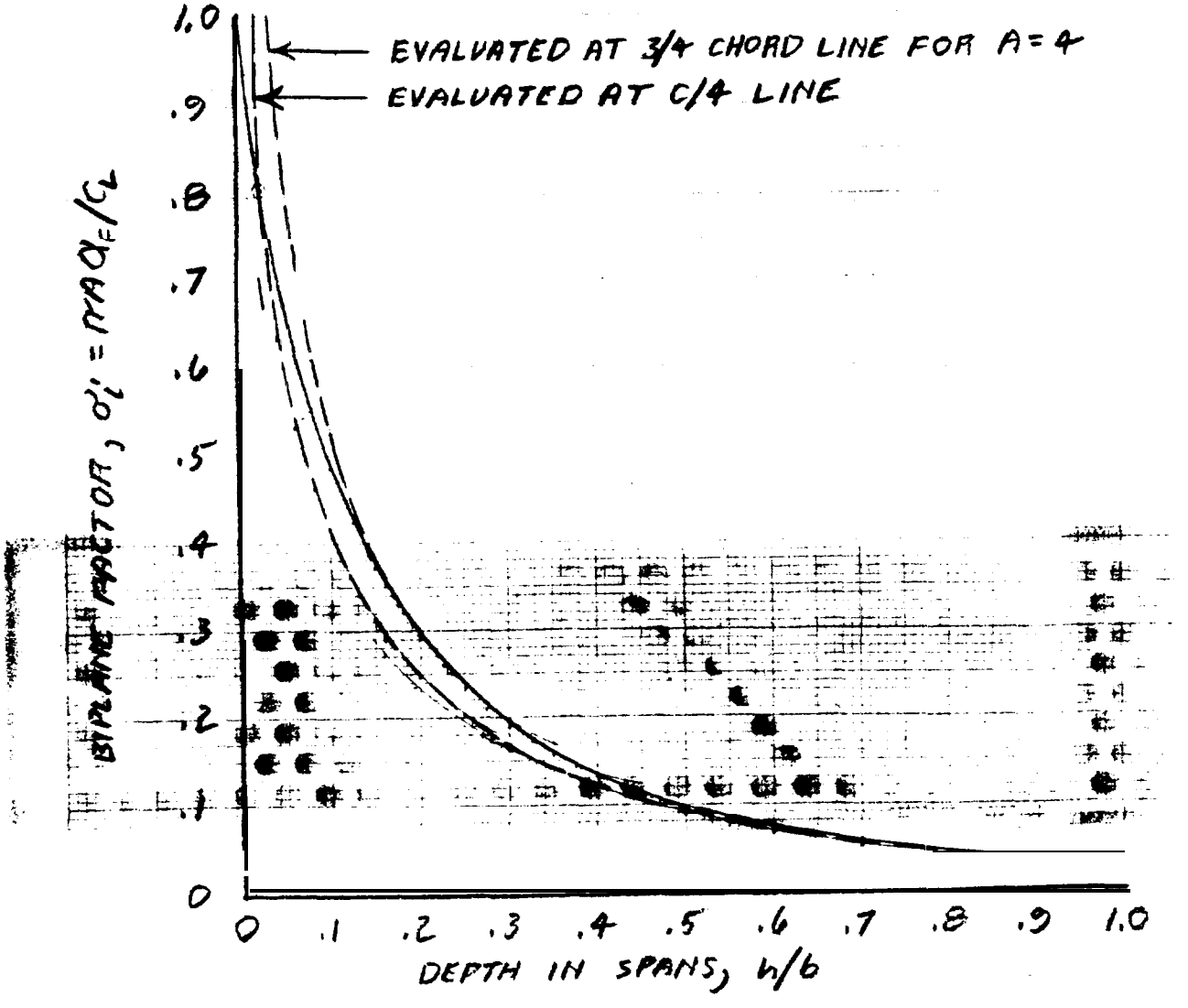

HRW 4/13/84

FIG. 3.5.6-5

GIBBS & COX WAVE DRAG APPROXIMATION

A = 6

$$K = \left(\frac{C_W}{C_L^2} - 2\frac{\sigma_i'}{\pi A}\right) \Big/ \frac{f(F_h)}{h/c}$$

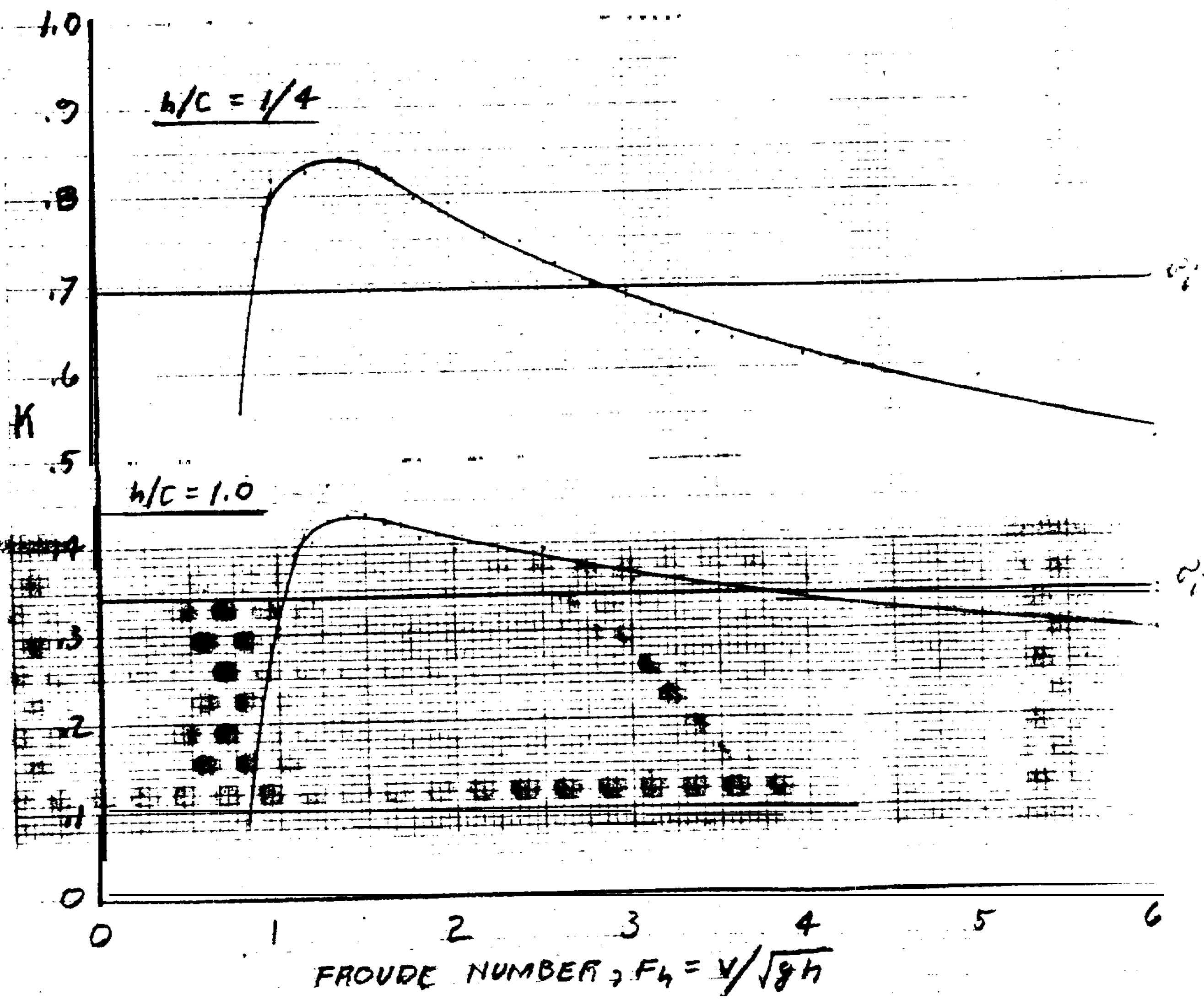

HAW 7/3/84

FIG. 3.5.6-6

FREE SURFACE DRAG

A = 6

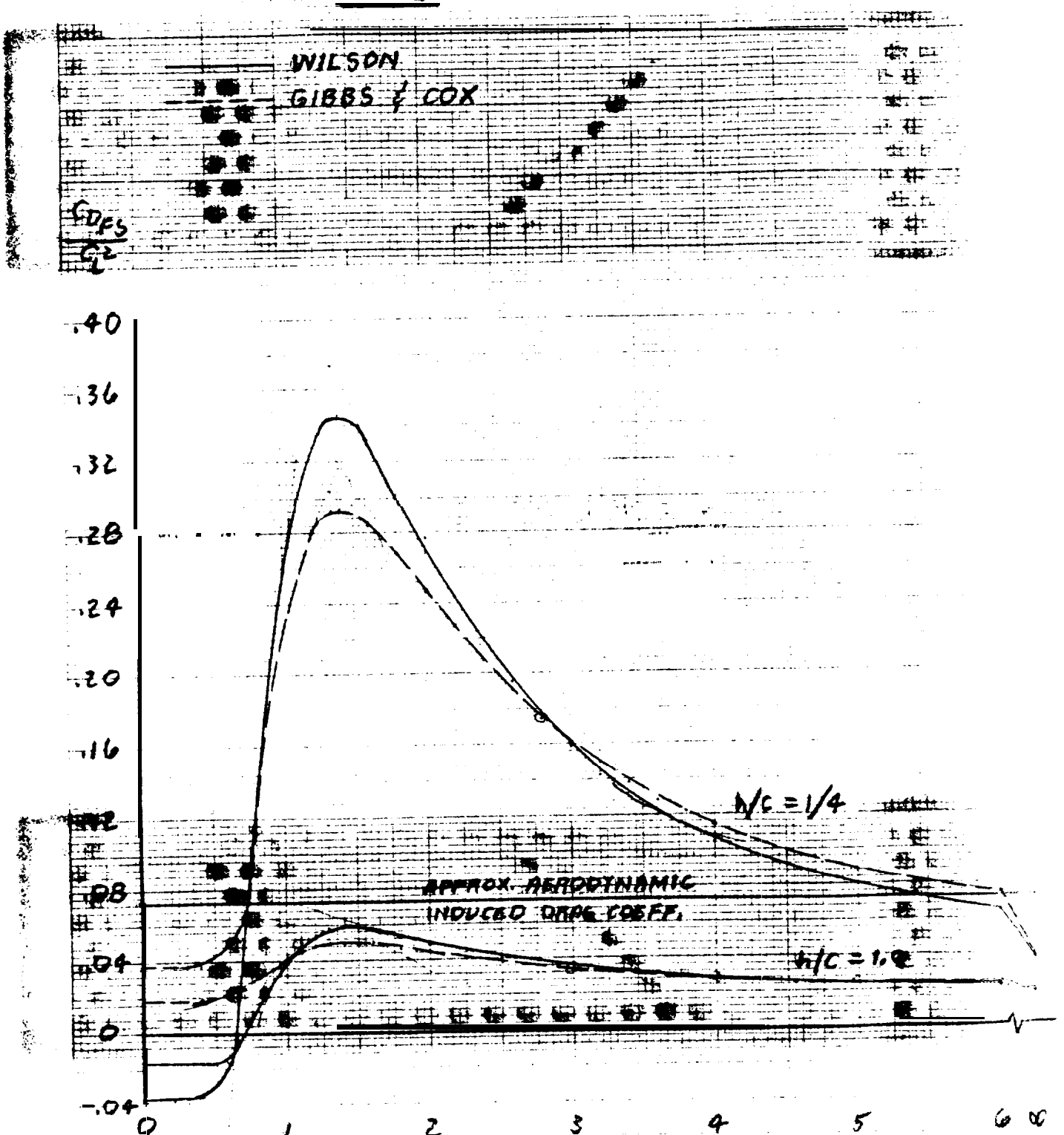

HAW 7/3/84

3.5.7 Foil Lift Equation

CLASSIC

From Equations 3.5.6-2, -4, -7, and -10 the inverse of the hydrodynamic lift curve slope is:

$$\alpha_{C_{L_{foil}}} = \text{section } \alpha + \alpha_{i_\infty}' + \alpha_{C_{L_C}} + \alpha_{i_{surf}}' + \alpha_{i_{wave}}' \qquad 3.5.7\text{-}1$$

where: section α = $1/2\pi K$

α_i' = aerodynamic induced angle, $C_i'/2\pi KA$

$\alpha_{C_{L_C}}$ = image bound vortex curvature (camber) effect

$$= \left[\sqrt{(4\tfrac{h}{c})^2+1+4A^2} - \sqrt{(4\tfrac{h}{c})^2+1}\right] \Big/ 4\pi A\left[(4\tfrac{h}{c})^2+1\right]$$

$\alpha_{i_{surf}}'$ = image free vortex biplane image induced angle

$$= \sigma_i'/\pi A$$

$\alpha_{i_{wave}}'$ = wave induced angle

$$= \sigma_i' f(F_h)/\tfrac{h}{c}$$

Equation 3.5.7-l is essentially Equation (2.34) of Reference 1 and two limitations should be noted:

- The viscous effect is defined only for the aerodynamic terms.
- The curvature correction is for a uniform circulation distribution, the "surface image" term is for an elliptic circulation distribution, and the "wave" term is derived without reference to the circulation distribution. This limitation is particularly significant to the incidence and flap lift cases which present relatively distorted circulation distributions.

Potential theory provides an adequate approximation for the pod lift increment:

$$\Delta C_{L_{\alpha_{pod}}} = 2 S_{o_{pod}} / S \qquad 3.5.7\text{-}2$$

where $S_{o_{pod}}$ = pod frontal area

Then the hydrodynamic lift curve slope is given by:

$$C_{L_\alpha} = C_{L_{\alpha_{foil}}} + \Delta C_{L_{\alpha_{pod}}} \qquad 3.5.7\text{-}3$$

which is essentially the hydrodynamic equivalent of the aerodynamic procedure of Reference 2.

AN ALTERNATIVE APPROXIMATION

By analogy with the aerodynamic case the hydrodynamic foil lift curve slope can be constructed from the hydrodynamic section lift curve slope of Equation 3.3.7.1-19 and the potential foil lift curve slope of Equation 3.4.1.1-2 in the form:

$$C_{L_{\delta_1 foil}} = K\, C_{L_{\delta_1 pot}} \qquad 3.5.7\text{-}4$$

where: $K = \dfrac{c_{l_{\alpha RN}} / c_{l_\alpha}}{c_{l_\alpha} / c_{l_{\alpha M}}} H \dfrac{c_{l_\alpha}}{c_{l_{\alpha\infty}}}$

$c_{l_{\alpha RN}} / c_{l_\alpha}$ = Reynolds number correction of Equation 3.3.1.1-1 or -2

$c_{l_\alpha} / c_{l_{\alpha M}}$ = Mach number correction of Equation 3.3.1.1-3

H = Section viscous lift curve slope correction of Equation 3.3.1.2-10

$c_{l_\alpha} / c_{l_{\alpha\infty}}$ = section hydrodynamic lift curve slope correction of Equation 3.3.7.1-19

$C_{L_{\delta_1 pot}}$ = Potential foil lift curve of Equation 3.5.5-1.

In comparison with the Gibbs and Cox equation, Equation 3.5.7-4 neglects the surface image induced angle and over-emphsizes the wave induced angle. For an infinite Froude number the two equations are compared as a function of

depth on Figure 3.5.7-l and as a function of aspect ratio on Figure 3.5.7-Z. In spite of these deficiencies in form, Equation 3.5.7-4 is selected for the Specification Volume in Section 3.5.8 of this volume.

HANDE

The three dimensional free surface lift curve slope effect of Reference 3 may be written:

$$\frac{C_{L\alpha}}{C_{L\alpha_\infty}} = \frac{C_{L\alpha_{F_h=\infty}}}{C_{L\alpha_\infty}}\left[1-.7423\,e^{-\sqrt{h/c}\left(.544\sqrt{h/c}+.433F_h\right)}\right] \qquad 3.5.7\text{-}5$$

where $$\frac{C_{L\alpha_{F_h=\infty}}}{C_{L\alpha_\infty}} = 1-\frac{1}{2}\left(\frac{h/c}{.7+.025A}+1\right)^{-2}-\frac{.031809}{A}\left(\sqrt{\frac{A^2}{K^2\cos^2\Lambda}+4}+2\right)$$

The HANDE equation is of emperical form which precludes identification of bound and free image vortex and Froude number effects: thus the equation cannot distinguish these effects in experimental data and can only be compared with other equations in terms of the total free surface effect for particular cases. It is also possible that the HANDE equation includes Reynolds number effects in the data base from which it was derived.

REFERENCES

1. Michel, W.H., S.F. Hoermer, L.W. Ward, and T.M. Buermann, "Hydrofoil Handbook Vol. II, Hydrodynamic Characteristics of Components," Bath Iron Works Corp. by Gibbs & Cox, Inc., 1954.
2. Pitts, W.C., J.N. Nielsen, and G.E. Kaattari, "Lift and Center of Pressure of Wing-Body-Tail Combinations at Subsonic, Transonic, and Supersonic Speeds," NACA Report 1307, 1959.

3. "Hydrofoil Analysis and Design Program (HANDE) Theory Manual," Vol. II, Boeing Company Document No. D321-51312-2, 2 July 1978.

FIG. 3.5.7-1

LIFT CURVE SLOPE COMPOSITION

ELLIPTICAL CIRCULATION DISTRIBUTION

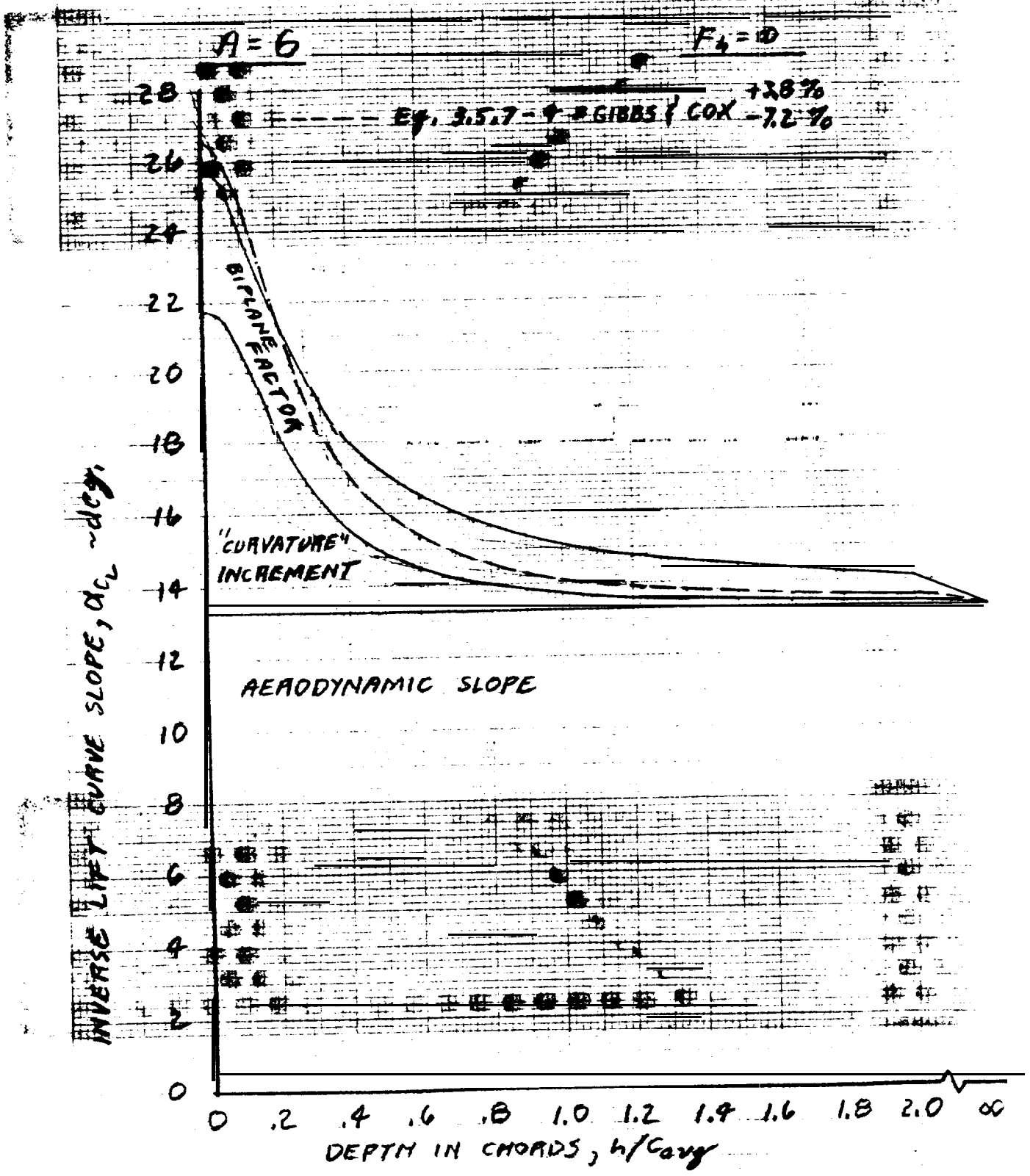

HRW 7/6/84

FIG. 3.5.7-2

LIFT CURVE SLOPE COMPOSITION

ELLIPTICAL CIRCULATION DISTRIBUTION

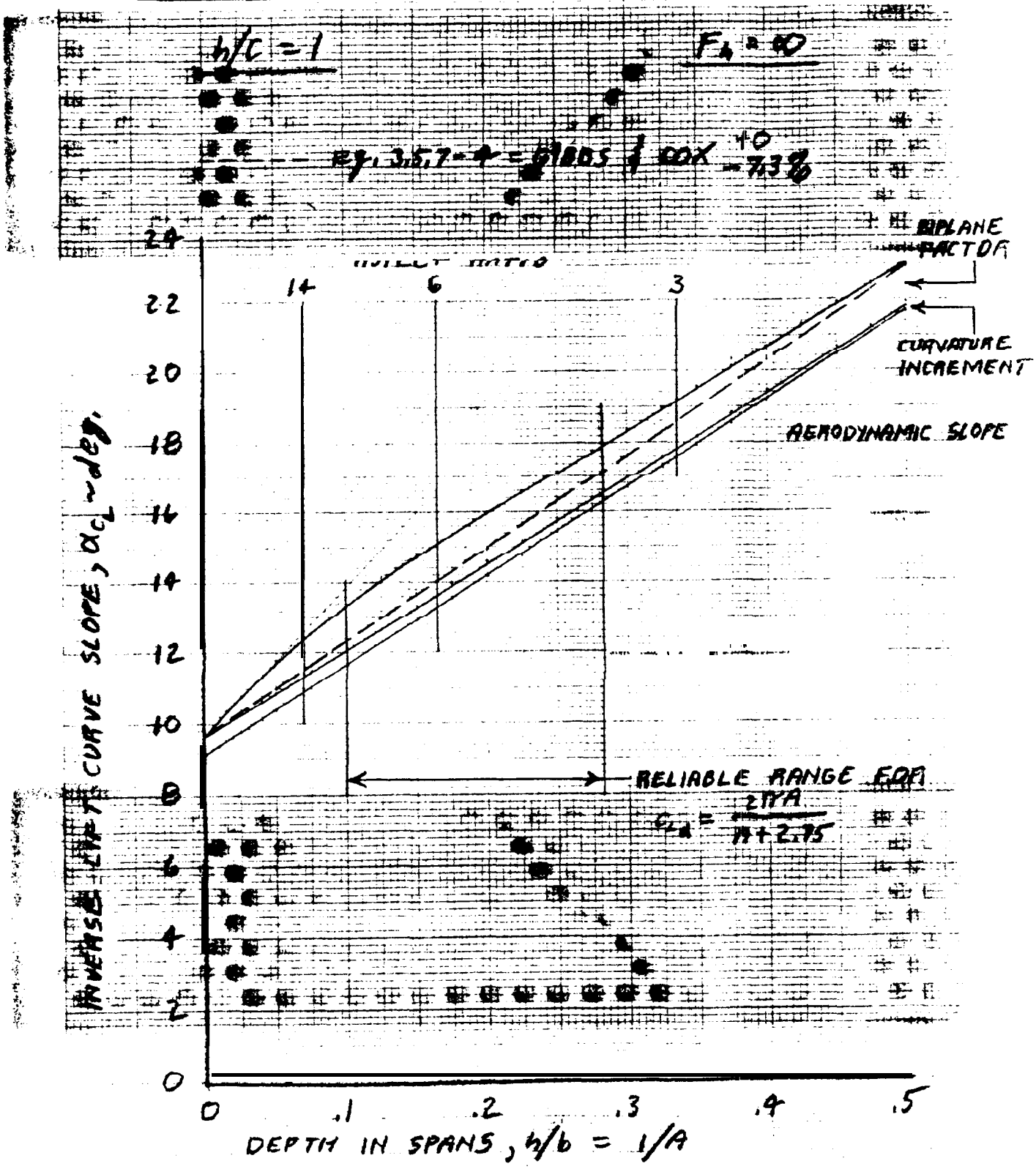

HMW 7/6/84

3.5.8 Experience

WADLIN DATA

Reference 1 presents a well planned comprehensive experimental study of free surface lift effect which, nevertheless, illustrates the difficulties encountered in this type measurement. Rectangular models of aspect ratio 4 and 10 were tested. The aspect ratio 10 foil was mounted without fillers at the bottom of a rectangular strut; the aspect ratio 4 foil was sting mounted. The foil section was 64,A412. The aspect ratio 10 foil was tested in two tanks of different cross section. The tank dimensions and tested conditions are given in Table 3.5.8-I.

Wadlin's measured zero lift angles are presented on his Figure 10 where the variation with Reynold's Numbers below $.5 \times 10^6$ has only speculative significance. For all significant Reynolds Numbers the zero lift angle was -3.3' for both models in both tanks at maximum and minimum depth. This measurement is nominal as shown on Figure 3.5.8-l by comparison with Equation 3.3.1.3-2 and with the 64A Series section values of DATCOM Table 4.1.1-B. It is particularly interesting to note that the strut had no significant effect upon the zero lift angle.

One of the more troublesome problems in the interpretation of hydrodynamic data in the absence of aerodynamic data for the same configuration is the establishment of the section lift curve slope variation with Reynolds Number. This effect introduces a systematic speed dependency comparable with that for free surface effect, Equations 3.3.1.1-l and -2, which give the expected variation of section lift curve slope with Reynolds Number, are derived from all of the lift curve slopes of Reference 2 but still present: a limited view

with significant exceptions. Two sections similar to Wadlin's are compared with Equation 3.3.1.1-1 on Figure 3.5.8-2. Also included on Figure 3.5.8-2 is the 65_3-418 variation of Wadlin's Figure 10 which is referenced to its value at the 2×10^6 Reynolds Number for the ratio presentation of Figure 2; i.e., the variation might be shifted vertically on Figure 3.5.8-2. The figure would indicate that the Wadlin data is subject to Equation 3.13.1.1-l but requires data djustments of the order of the free surface effect under study.

Measurement of the experimental slope presents a second major problem in the data reduction process. Hydrodynamic model lift curves are subject to a number of distinct non-linearities and to the usual experimental random error. Measurement of the lift curve slope is therefore subjective to some extent and a ±5% scatter is not unusual. The scatter can be reduced by reviewing the measure of selected slopes but such selection inevitably leads in the direction of a prejudged effect.

The significance of the measurement problem is shown on Figure 3.5.8-3. Wadlin's Figure 5 presents the measured data points and the lift curve slope measurements from that figure were made for Figure 3.5.8-3 here. These measurement5 smoothed the data by giving greatest weight to the lower lift points to avoid cavitation influence, therefore these measurements introduce subjective random and systematic bias. It should be noted that Wadlin calls the data "cavitation free." Time did not allow derivation of the theoretical cavitation bucket for the models.

Wadlin's Figure 7 presents his interpretation of the lift measurements which still contain high lift coefficient non-linearities characteristic of cavitation. The slopes of Figure 3.5.8-3 are therefore interpretations of his interpretations which were made for a much earlier study of this data. Note that a systematic variation of lift curve slope with speed is much more evident

in the Figure 5interpretations and this characteristic is crucial to the objective of the test program. Wadlin's Figure 10 presents his interpretation of his Figure 7 which is practically identical with that of this analysis.

Figure 3.5.8-4 addresses the question of the reliability of the lift curve slope as measured on Wadlin's Figure 5. The indication here is that at high speed, where the lift force is large, there is no significant difference between the lift curve derived directly from the forces and that derived from the lift coefficients. At low speed, however, the accuracy afforded by Wadlin's Figure 5 does not provide a significant lift curve defintion. Thus lift curves read from Wadlin's Figure 7 provide the best measure of the test results.

Tank boundary effects are not usually a model data consideration but comparison of Wadlin's Tank No. 1 and Tank No. 2 results requires consideration of this effect. The tank boundary effect employed here was:

$$\frac{C_{L_\alpha}}{C'_{L_\alpha}} = 1 + \frac{K_\Delta}{1 + \frac{A}{C_{l'}}} \qquad 3.5.8\text{-}1$$

where: C_{L_α} = lift curve slope in tank of infinite width and depth

C'_{L_α} = lift curve slope in tank of finite width and depth

$K_{\Delta W}$ = finite width effect = $.1/[.16 - (B/b)^2]$

$K_{\Delta B}$ = finite depth effect = $-\sigma'_1 = f(d/b)$

A = aspect ratio

$C_{l'}$ = aerodynamic induced angle coefficient of Equation 3.5.5-12

b = foil span

B = tank Width

d = model distance fron tank bottom

K_Δ = $K_{\Delta W} + K_{\Delta B}$ (for practical cases and note that K_Δ has a

negative value)

Wadlin presents the tank boundary effect graphically on his Figure 14 but Equation 3.5.8-l was employed because Wadlin's figure was so difficult to read. Wadlin's tank boundary effect does appear to be some 50% greater than that of Equation 3.5.8-1, as shown on Figure 3.5.8-5, but that difference did not become significant to the data analysis.

From Figure 3.5.5-l for a 2π section lift curve slope, the potential aerodynamic lift curve slope expected for the two models is:

$$C_{L_{\alpha_{pot}}} = \frac{2\pi \times 10}{13.1} = 4.7963 \text{ for } A=10$$
$$= \frac{2\pi \times 4}{7.05} = 3.5649 \text{ for } A=4 \qquad 3.5.8\text{-}2$$

From Table 3.3.1.2-X: the expected section lift curve slope is:

$$K = 1-.49x12-.97(.12)^2 = .92680 \qquad 3.5.8\text{-}3$$

and the viscous aerodynamic lift curve slope expected for the two models is:

$C_{L_{\alpha_{\alpha}}}$ = .9268x4.7963 = 4.4 452 for A=10 3.5.8-4

= .9268x3.5649 = 3.3040 for A=4

Wadlin's deepest depth lift curve slopes, reduced by the tank wall effects of Equation 3.5.8-1, are compared with the lift curve slopes of Equation 3.5.8-4 on Figure 3.5.8-6. Reference to Figures 3.3.1.2-3 and 3.5.5-1 shows that the results lie well outside aerodynamic experience for the section or foil lift curve slope. The tank wall effect adjustment correlated the aspect ratio 10, Tank 1 and 2 results well. There is an unexpected clear indication that the aspect ratio 4 results are not subject to Reynolds Number effect.

From Figure 3.5.8-6 the aerodynamic characteristics are assumed to be:

A=10; $C_{L_{\alpha}}$ = $4.4.452+.1867\ RN \times 10^{-6}$ for RN $\leq$ 3x106 3.5.8-5

A=4; $C_{L_{\alpha}}$ = 3.7203

This result is 12.6% higher than expected and clouds interpretation of the free surface effects obtained.

Wadlin's zero lift angles and lift curve slopes were measured on his Figures 6 and 7 with the results shown in Tables 3.5.8-11 and -111. In the tables the measured lift curve slopes have been reduced by the estimated tank boundary effect and referenced to the aerodynamic slopes of Equation 3.5.8-5 to obtain the measured $C_{L_\alpha}/C_{L_{\alpha_\infty}}$ and the results are shown as a function of Froude Number on Figures 3.5.8-7 and -8 where the results are compared with the Gibbs & Cox equation, Equation 3.5.7-1, and with Equation 3.5.7-4.

Except for the aspect ratio 10 model at shallow depth and for Froude Numbers of 4 or less, the Wadlin data gives no indication of a Froude Number effect and the range of measured lift curve slopes for each model and depth can be taken as a measure of the infinite Froude Number lift curve slope as on figure 3.5.8-9 where the result constitutes a summary of the Wadlin data. Wadlin's measured ratios on Figure 3.5.8-9 are from Figure 15 of Reference 1 and combine independent measurements of the experimental data with independent estimates for the aerodynamic slopes. The comparison of the two independent interpretations' on the figure is probably typical for hydrodynamic data.

In section 8.2.2.4 of Reference 3 the infinite Froude Number hydrodynamic slope of Equation 3.5.7-5 is given in the form

$$\frac{C_{L_{\alpha_{F_n=\infty}}}}{C_{L_{\alpha_\infty}}} = 1 - \frac{1}{2}\left(\frac{h/c}{\pi t.025A}+1\right)^{-2} - .00936\left|\lambda - .2\right| / C_{L_{\alpha_\infty}} \qquad 3.5.8\text{-}6$$

The final term of this equation is substantial for rectangular foils and accounts for the low position of the HANDE predictions on Figure 3.5.8-9. Note that the HANDE aerodynamic slope on Figure 3.5.8-9 is about 18% lower than nominal for these planforms. Because rational equations typical Jy underestimate the hydrodynamic lift curve slope and because emperical equations cannot

contribute to an explanation for that fact, the HANDE equation is not included in the remaining experimental reviews of this section.

There is qualitative indication of a Froude Number effect on Figure 3.5.8-7 and weaker qualitative evidence of an aspect ratio effect on Figure 3.5.8-9 but the entire set of data infers an incredible aerodynamic slope and does not really distinguish between the predictions even as to form.

PCH MODEL AND PROTOTYPE DATA

Layne reports the results of towing tank tests of the DTMB PCH forward foil model and of a 64A309 section version of that model in Reference 4. The 16-309 section model had been designed for Froude scaled speeds and testing was discontinued when excessive flap distortion was encountered at higher cavitation scaled speeds.

Only the zero flap results are considered here. Layne adjusted the 16-series section lift results to the zero incidence of the 64A series section model. Here that adjustment is reversed to make both sets of results comparable with the prototype. In addition the 64A series section lifts were adjusted for the difference between the lift curve slope factors, a , for the two sections. The lift curve slope variation with Reynolds Number at the deepest test depth, 1 chord for the 16-series section and 2 chords for the 64A series section, was consistent with Equation 3.3.1.1-1 and all of the lift curve slopes were adjusted to a Reynolds Number of 3×10^6 by that equation for comparison with the prototype data.

The predicted aerodynamic lift curve slope for the prototype is:

$$c_{l_\alpha} = .2509 + .07627 (\alpha^\circ + .481105^\circ) \qquad 3.5.8\text{-}7$$

$$\alpha_{c_l = 0} = -3.2901^\circ$$

Figure 3.5.8-10 presents the variation of the model zero lift angle with speed. Adjusting Layne's zero incidence angles to the prototype incidence introduced an uncertainty into this measurement but that uncertainty is not a function of speed. No classical Froude Number effect will account for this variation of zero lift angle with speed, which however, is in the direction of the structural wash-out associated with the moment about the aerodynamic center. The model zero lift angle is at least I/2 degree lower (more negative) than predicted while the prototype zero lift angle is at least I/2 degree

higher. The nominal uncertainty associated with this angle is 1/3 degree for the section in Equation 3.3.1.3-2.

Figure 3.5.8-11 compares the model lift curve slope variation with Froude number with that of Gibbs & Cox and Equation 3.5.7-4. The theoretical Froude Number variations are related to the deepest depth measured slope rather than to the predicted aerodynamic slope. The measured variation with Froude Number is the reverse of the theoretical variation and particularly so for the 16-series section model. Presumably this is a dynamic pressure, rather than Froude Number, effect and attention was therefore shifted to the lowest speed data.

Figure 3.5.8-12 compares the model variation of lift curve slope with depth with that of Gibbs & Cox and Equation 3.5.7-4. Two possible interpretations of the prototype data, discussed below, are also shown. The Gibbs & Cox equation describes the model best while Equation 3.5.7-4 describes the prototype best; which is to say that this experience will not distinguish between the two equations.

The prototype data is compared with Equation 3.5.8-7 on Figure 3.5.8-13. Alternative values for the zero lift angle, lift curve slope, and $C_{L\delta}/C_{L\alpha}$ ratio derived from a 3-variable linear regression are also shown. The limited craft pitch range available to the prototype cannot define the $C_{L\delta}/C_{L\alpha}$ ratio closer than about 15%. For academic purposes it would be desirable to have a better full scale measurement of this ratio but the predicted value is fully adequate to the prototype for all practical purposes.

In summary, aerodynamic theory with Equation 3.5.7-4 describes the PCH model and prototype zero lift angle within 1/2 degree and their lift curve slopes within 11%. The two equations cannot be distinguished by the model and

full scale data and both represent the prototype better than the model does and, in fact, the prototype data cannot distinguish any free surface effect.

AG (EH) MODEL AND PROTOTYPE DATA

For this case all model and prototype data was adjusted to the DTMB main foil model section as required and the predicted lift curve was:

$$C_{L_\alpha} = .095151 + .049336(\alpha^\circ + .79911^\circ) \qquad 3.5.8\text{-}8$$

$$\alpha_{C_L=0} = -1.9286^\circ$$

The data detailed here is the main foil model data of Reference 5 which ranged over pitch and incidence with fixed transition and the prototype data of References 6 and 7. As for the PCH forward foil, the lift curve slope and zero lift angle are functions of the $C_{Li}/C_{L\alpha}$ ratio. For the model data 3-variable regressions were employed and the $C_{Li}/C_{L\alpha}$ ratios noted, for the prototype data 2-variable, with the predicted $C_{Li}/C_{L\alpha}$, and 3-variable regressions were employed.

The measured zero lift angles are compared with the prediction on Figure 3.5.8-14. The model and prototype measurements range over 1/2 to 3/4 degrees with the prediction on the lower (most negative) end of that range.

The measured lift curve slopes are compared with the predicted slope on Figure 3.5.8-15 which details data obtained by pitch and incidence sweeps on configurations which are identical except for camber. That detail shows theory and model about 12% under the prototype slope. Now the aft foil data of Reference 5, the data of Reference 8, and unpublished whirling tank data for the main foil all measure the same characteristic with identical or virtuallyidentical configurations with results which are centered 11% above the prototype measurements.

In this case then, the aerodynamic theory provides a much better prototype prediction than does hydrodynamic theory or model measurement. Of course the addition of a substantial body of prototype data might change this conclusion.

SHIMRIT MODEL AND PROTOTYPE DATA

The SHIMRIT forward foil system lift characteristics are known only by Grumman whirling tank tests of the FLAGSTAFF foil system and by prototype measurements on two voyages. The mode7 was identical with the prototype except for aspect ratio which was 6.0 for the mode7 and 5.5 for the prototype. The incidence angle for this foil system is fixed so the $C_{Lt}/C_{L\alpha}$ ratio does not influence thelift curve slope

Because the data is limited in this case the data analysis is presented in a little more detail to introduce some of the practicalities in the prediction and measurement of the lift curve.

Figure 3.5.8-16 presents the prototype measurements of the lift curve. The lift curve was measured on many voyages but these were theonly two for which there was no obvious reason in the instrumentation, procedure, sea state, or results for discarding the data. Thus this data has already passed through a screen which is subjective to some extent.

The lift coefficient range of Figure 3.5.8-16 is practical; providing a range adequate to the definition of the lift curve slope would require extreme ranges of craft weight and C.G. The subjective nature of a straight line drawn through this data is not quite so obvious if the line is drawn by linear regression analysis rather than by eye. On figure 3.5.8-16 two such lines, bounding the 90% confidence interval for slope, are drawn through the mean C_L and α for comparison with the predicted lift curve. Analytically that comparison is:

Predicted $C_{L_\alpha} = .10351 + .068119\alpha^\circ$; $\alpha_{C_L=0} = -1.520^\circ$ 3.5.8-9

Measured $C_L = .10347 + .074862\alpha^\circ$; $\alpha_{C_L=0} = -1.382^\circ$ 3.5.8-10

The measurements at lift coefficients higher than .35 on Figure 3.5.8-16 must be assumed to be subject to substantial cavitation. They were included in the linear regression because their omission produced a zero lift angle and slope which differed from theory by amounts far exceeding previous experience. The result is entirely satisfactory intuitively because these six points have a relationship to the "measured" wetted lift curve which is characteristic of heavy cavitation at low speed. Similar examinations of individual points was extremely tedious for the AGEH and PCH where the C_{L_F}/C_{L_α} and $C_{L_\delta}/C_{L_\alpha}$ ratios were an added uncertainty. In the case of the PCH, however, a substantial body of visual cavitation observations eliminated some of the subjectivity from the process.

Figure 3.5.8-17 compares the prototype and model zero lift angles with the predicted value. Only the model measurement at the 1.65 chord depth exceeds the nominal 1/3 degree uncertainty for this characteristic for the section. The effect of eliminating the six points of highest lift coefficient from the prototype linear regression is indicated.

Figure 3.5.8-18 compares the prototype and model lift curve slopes with the predicted value. When the adjustment of Equation 3.3.1.1-l is made for the half-million model Reynolds Number the result is 30% higher than the predicted aerodynamic slope which puts the model measurement in doubt. The prototype measurement may be described as agreeing with the prediction within the limits of the experimental accuracy, for almost any theoretical free surface effect.

The SHIMRIT experience provides no conclusive evidence that there is a free surface effecton the lift curve slope, much less distinguishing between estimates for that effect.

SUMMARY OF EXPERIMENTAL DATA

Table 3.5.8-IV summarizes the prototype experience considered here. The table is directed to two questions:

How reliable is the lift curve prediction for the prototype?

How much confidence does model testing lend to thelift curve prediction?

Obviously experience provides no quantitative answers for these questions and only tentative qualitative answers. In general the predicted lift curve slope is low, by as much as 17%; the predicted zero lift angle is high (less negative), by as much as a degree; and the predicted foil angle for practical lift coefficients is high, by as much as 1½ degrees. Model tests appear to increase the uncertainty associated with the lift curve. This observation is discussed below but it must be noted here that the poor precision of the model relative to the prototype in Table 3.5.8-IV reflects, to some degree, the fact that much more data is available for the model than for the prototype.

Note that foil drag, moment, and cavitation are essentially functions of lift and lift distribution; foil, incidence, and flap angles are peripheral design considerations. Thus the lift curve uncertainty need not have any particularly significant effect upon craft performance and this volume has consistently isolated the lift distribution and lift curve uncertainties. The lift curve uncertainty does suggest generous incidence angle quadrants and incidence adjustment provision for flap lift systems.

The major prototype measurement problems are the limited lift coefficient range and the difficulty in providing precise depth control over a significant range of depths. Nevertheless confidence in the lift curve prediction must await a prototype test program dedicated to overcoming these limitations.

The primary model measurement problem is the Reynolds Number effect problem with some indication that different hydrodynamic facilities present distinctive effective Reynolds Numbers. Free surface facilities leave some question about the aerodynamic lift curve under the best circumstances, suggesting supporting tests in the water tunnel or wind tunnel. Model distortion under load is a continuing problem which is allieviated by lower test speeds only at the expense of Reynolds Number problems. Internal strut ventilation has been a recognized problem in flap lift tests and a suspected problem in some incidence lift tests.

Wind tunnel testing has not received due attention in hydrofoil studies. Wind tunnels have the advantage of substantially more resources than are available to hydrodynamic facilities, particularly in the area of cross correlations with other facilities and with prototyoes. Many of the hydrodynamic model problems are peculiar to the fluid density. For the foreseeable future the wind tunnel would provide a valuable reference point for any hydrodynamic experimental study and the best available measure of the prototype lift curve for all practical purposes.

For maximum general benefit for the limited resources available to the hydrofoil, each experimental program should be set into some well defined context which identifies each compoment of the lift curve. Table 3.5.8-IV contains only a fraction of the experimental data already available and is not adequately systemtized for the general purpose.

In summary, the free surface depth effect is known experimentally but only qualitatively; the best correlation available here, that for Gibbs & Cox on Figure 3.5.8-12, has eliminated 25% of the model data and is compromised by the prototype data. Froude Number effect is not available to the prototype and none is evident in the model data. Therefore, while inadequate in form,

Equation 3.5.7-4 is adopted here for the lift curve slope because it is indistinguishable from the Gibbs & Cox equation in the existing state of the art and is much more convenient in practice. In fact, it is not likely that the prototype lift curve will be distinguished from the aerodynamic lift curve in the foreseeable future.

REFERENCES

1. Wadlin, K.L.; C.L. Shuford, Jr.; and J.R. McGehee; "A Theoretical and Experimental Investigation of the Lift and Drag Characteristics of Hydrofoils at Subcritical and Supercritical Speeds", NACA Report 1232, 1955.
2. Loftin, Jr., L.K. and H.A. Smith, "Aerodynamic Characteristics of 15 NACA Airfoil Sections at Seven Reynolds Numbers from 0.7 x 10^6 to 9.0 x 10^6," NACA Technical Note 1945, October 1945.
3. "Hydrofoil Analysis And Design Program (HANDE) Theory Manual," Vol. II, Boeing Company Document No. D321-51312-2, 2 July 1978.
4. Layne, Douglas E., "Lift And Drag Characteristics of NACA 16-309 and NACA 64A309 Hydrofoils", DTNSRDC Report SPD-326-07, October 1976.
5. Richter and Palmer, "AG(EH) Hydrofoil Research Ship Hydrodynamic Report of Model Test Program," GAC Report M23.77, 21 August 1962, as amended 15 January 1963.
6. Rand, A.H., "Contract N00600-69-C-0618 (Phase IV), AGEH-1 HYSTU Plan BE132-A241, Transmittal of Trim Data," Boeing Letter 2-1524-1000-753 to Commander, NSRDC, et.al., 19 October 1972.
7. Wright, W.E., "Post-RAV Foilborne Trial Results," Plainview (AGEH-1) Technical Note TN-A-8, Nov. 1971.
8. Spangler, "Model Test Results for the HYSTAD Strut-Nacelle-Foil Combination," NSRDC Report2138, January 1966.